Agricultural and Forest Meteorology 328 (2023) 109256

Contents lists available at ScienceDirect

Agricultural and Forest Meteorology

journal homepage: www.elsevier.com/locate/agrformet

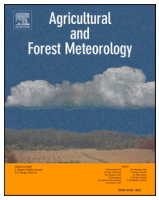

The role of radiative cooling and leaf wetting in air–leaf water exchange during dew and radiation fog events in a temperate grassland

Yafei Li [a,*], Andreas Riedl [a], Werner Eugster [a], Nina Buchmann [a], Lucas A. Cernusak [b], Marco M. Lehmann [c], Roland A. Werner [a], Franziska Aemisegger [d]

[a] Institute of Agricultural Sciences, ETH, Zurich 8092, Switzerland
[b] Centre for Tropical Environmental and Sustainability Science, College of Science and Engineering, James Cook University, Cairns, Queensland 4878, Australia
[c] Forest Dynamics, Swiss Federal Research Institute for Forest, Snow and Landscape Research (WSL), Birmensdorf 8903, Switzerland
[d] Institute for Atmospheric and Climate Science, ETH, Zurich 8092, Switzerland

ARTICLE INFO

Keywords:
Dew and fog
Radiative cooling
Leaf wetting
Leaf temperature
Stable isotopes
Dry and hot summer

ABSTRACT

During prolonged dry periods, non-rainfall water (NRW) plays a vital role as water input into temperate grasslands, affecting the leaf surface water balance and plant water status. Previous chamber and laboratory experiments investigated air–leaf water exchange during dew deposition, but overlooked the importance of radiative cooling on air–leaf water exchange because the chamber is a heat trap, preventing radiative cooling. To complement these previous studies, we conducted a field study, in which we investigated the effect of radiatively-induced NRW inputs on leaf water isotope signals and air–leaf water exchange in a temperate grassland during the dry-hot summers of 2018 and 2019. We carried out field measurements of the isotope composition of atmospheric water vapor, NRW droplets on foliage, leaf water, xylem water of root crown, and soil water, combined with meteorological and plant physiological measurements. We combined radiation measurements with thermal imaging to estimate leaf temperatures using different methods, and computed the corresponding leaf conductance and air–leaf water exchange. Our results indicate that radiative cooling and leaf wetting induced a switch of direction in the net water vapor exchange from leaf-to-air to air-to-leaf. The leaf conductance and air–leaf water exchange varied by species due to the species-specific biophysical controls. Our results highlight the ecological relevance of radiative cooling and leaf wetting in natural temperate grasslands, a process which is expected to influence land surface water budgets and may impact plant survival in many regions in a drier climate.

1. Introduction

During dry spells, non-rainfall water (NRW), mainly dew and fog, are additional water sources (besides rainfall water) for plants across many ecosystems (Dawson, 1998; Feild and Dawson, 1998; Agam and Berliner, 2006). However, little research has been done on the ecohydrological relevance of NRW inputs to temperate grasslands (Jacobs et al., 2006; Li et al., 2021). With global warming, dry seasons are predicted to become drier (IPCC, 2021), hence NRW is expected to have an increasing hydrological significance. Central Europe, with Switzerland included, is also expected to experience longer dry spells in the future (CH2018, 2018). Because NRW inputs are a key component of land-atmosphere exchange processes, occurring on approximately one third of the nights in a year in a typical Swiss grassland (Riedl et al., 2022), they are expected to become increasingly important for plant survival and growth during dry spells.

Hydrogen and oxygen stable isotopes ($^{18}O/^{16}O$ and $^{2}H/^{1}H$) are efficient and natural tools to trace water cycling (Dawson and Ehleringer, 1991; Ehleringer and Dawson, 1992) in the soil-plant-atmosphere continuum, hence they are used also to investigate the effect of dew (Wen et al., 2012) and fog (Dawson, 1998) on plants. The most important isotopologues of water in the hydrological cycle are $^{1}H_2^{16}O$ (major and light isotopologue), $^{1}H^{2}H^{16}O$ and $^{1}H_2^{18}O$ (minor and heavy isotopologues). Equilibrium and kinetic isotope fractionations occur during phase transitions due to the distinct saturation vapor pressure and diffusivity of the different isotopologues (Urey, 1947; Merlivat, 1978; Criss, 1999). The strength of daytime leaf water enrichment in strongly undersaturated conditions varies among different lifeforms due to

* Corresponding author.
E-mail address: yafei.li@usys.ethz.ch (Y. Li).

https://doi.org/10.1016/j.agrformet.2022.109256
Received 2 July 2022; Received in revised form 18 November 2022; Accepted 20 November 2022

species-specific Péclet numbers (Lai et al., 2008), which relate advective to diffusive transport in leaves. In contrast, in high-humidity environments, leaf water and atmospheric water vapor were found to rapidly reach the liquid–vapor isotope equilibrium (Helliker and Griffiths, 2007; Welp et al., 2008).

During clear and calm nights with a stable nocturnal boundary layer, radiative cooling in natural conditions causes leaf surfaces to cool down more than the near-surface atmosphere (e.g., by 0.9 °C cooler in Monteith, 1957), which induces dew formation on leaf surfaces. Radiative cooling is a prerequisite for dew and radiation fog nights to occur in nature. But in controlled experiments (Kim and Lee, 2011; Goldsmith et al., 2017; Gerlein-Safdi et al., 2018; Lehmann et al., 2018), even flow-through chambers can act as a heat trap preventing radiative cooling instead (Curtis, 1936). Furthermore, leaf wetting causes an increase in leaf emissivity (e.g., from 0.96 to 0.98 according to López et al., 2012), which enhances radiative cooling of wet leaf surfaces compared to dry surfaces (see Eq. (2) in Section 2.1). Therefore, the leaf–air thermal gradient in these laboratory experiments does not reflect field conditions, which, in turn, most likely affects the air–leaf vapor exchange. This aspect has mostly been overlooked by laboratory experiments assuming identical leaf and air temperatures, with bidirectional fluxes of isotopically depleted or enriched water occurring even without a net directed flux (Kim and Lee, 2011; Lehmann et al., 2018).

Dew and fog can improve the plant water status (Kerr and Beardsell, 1975; Boucher et al., 1995) through foliar water uptake (FWU) (Dawson, 1998; Pina et al., 2016; Berry et al., 2018; Dawson and Goldsmith, 2018; Schreel and Steppe, 2020), by taking up the dripping-off droplets via roots (Dawson, 1998; Holder, 2007), or by reducing leaf transpiration due to high humidity (Caird et al., 2007; Groh et al., 2019). Stomata are key pathways for FWU as compared to other pathways via cuticles, hydathodes and trichomes (Cape, 1983; Eller et al., 2013; Pina et al., 2016; Berry et al., 2018; Schreel and Steppe, 2020).

During dew and fog periods, the leaf conductance of wet leaves is difficult to be measured using most instruments (e.g., MeterGroup SC-1 leaf porometer, Licor LI-600P porometer, or Licor LI-6400/LI-6800 photosynthesis systems). Condensation on the instrument's humidity sensor under such conditions will lead to large uncertainties of measured results for leaf conductance. Eddy-covariance (EC) measurements with high time resolution are used to estimate leaf conductance (Bonan et al., 2014), but with dew or fog occurrences, the EC method tends to underestimate the latent heat flux by about 2/3 (Jacobs et al., 2006), and yields unrealistic values of latent heat flux if dew condenses on or fog droplets drip off on the optical window of the often employed open-path Infrared Gas Analyzer (Li et al., 2021). Furthermore, in contrast to the case of estimating leaf conductance during the evaporation process (i.e., a loss of water from internal leaf into the atmosphere), leaf conductance estimates during the condensation process with a net water transfer from atmosphere onto or into a leaf are much more challenging to obtain. The water exchange between internal leaf and atmosphere is further affected by plant physiological traits (e.g., leaf–root water potential gradients, and leaf water content). Hydraulic measurements are an option to obtain estimates of stomatal conductance for tree and shrub species (Bonan et al., 2014; Li et al., 2022), but it is difficult to measure sap flow of grassland species which are small and fragile. Soil–plant–atmosphere continuum models optimize water use efficiency (the ratio of CO_2 assimilation to water loss) to simulate leaf conductance (Bonan et al., 2014), which is an approach that is not applicable for the simulation of nighttime leaf conductance due to the absence of CO_2 assimilation. Thus, water isotopes present valuable additional observable constraints to assess the leaf's humidity budget in conditions close to ambient saturation at night. Based on an isotope mass balance, Kim and Lee (2011) computed that total leaf conductance (g_L) of crops exposed to simulated dew was 35–87 mmol m^{-2} s^{-1} in a chamber under dark conditions. However, the isotope mass balance method for computing g_L for wet leaves, to the best of our knowledge, has not been applied under field conditions yet.

Leaf temperature is important for understanding leaf thermal traits and the leaf–air water exchange. Leaf temperature is affected by leaf characteristics including leaf angle, size, conductance, and environmental conditions such as sunlight, humidity and wind speed (Foster and Smith, 1986; Gutschick, 2016; Muir, 2019). Moreover, with dew and fog formation, leaf temperature cools down via radiative cooling, and is warmed by the heat release via condensation (Monteith, 1957), while droplet evaporation after sunrise can induce evaporative cooling of leaf surfaces (Dawson and Goldsmith, 2018). At steady state under well-controlled conditions, leaf temperature simulation is accurate (Schymanski and Or, 2017) using the leaf energy budget, with leaf conductance as the input for modeling (Foster and Smith, 1986; Gutschick, 2016; Muir, 2019). However, it is a challenge to simulate the leaf energy balance under a dynamic environment (Vialet-Chabrand and Lawson, 2019). Leaf temperature can be measured by the methods of thermal resistance, thermocouple, infrared temperature, and infrared thermal imaging (Yu et al., 2015). Among these measurement methods, thermal imaging has an advantage for contactless and large-scale measurements, but the accuracy can be affected by emissivity, leaf-instrument distance, environment temperature and atmospheric absorption. In this study, we tested different estimation methods of leaf temperature, either (1) by longwave radiation (for canopy surface temperature) measurements, or (2) by combined radiation and thermal imaging measurements (for among-species differences of leaf temperature).

With this study, we aim at addressing two important research questions on land–atmosphere water exchange during nights with stably stratified nocturnal boundary layers. We assess the ecohydrological relevance of NRW input for air–leaf water exchange using stable isotopes of water for two dry-hot summers 2018 and 2019 in Central Europe. To compare the results during NRW input nights with those obtained during nights without NRW inputs, we selected three representative NRW events in 2018, one NRW event in 2019, and one contrasting windy night without NRW inputs in 2019, during which intensive observation campaigns were carried out. We asked the following two questions:

Q1) How does NRW formation affect the leaf water isotope composition?

Q2) How do NRW inputs affect the air–leaf vapor exchange and leaf water status, and how do different leaf temperature estimations affect estimations of air–leaf vapor exchange?

To address Q1, stable isotopes of water were used to investigate the main drivers of leaf water isotope signals during NRW inputs, in comparison to the conditions without NRW inputs. To address Q2, we quantified the effect of radiative cooling and leaf wetting on air–leaf vapor exchange and its direction. We computed total leaf conductance (g_L) based on the non-steady state leaf water enrichment model by Farquhar and Cernusak (2005), and then quantified the nocturnal water vapor exchange between the leaves and the atmosphere. To investigate whether the leaf water status was improved by NRW inputs, leaf water potential (LWP) was compared under conditions with and without NRW inputs, and relative water content (RWC) was used for checking whether the leaf reached turgid water content with NRW inputs. Finally, we assessed the uncertainty of different leaf temperature simulations, and their effect on our estimates of air–leaf vapor exchange.

2. Materials and methods

2.1. Study site

The Chamau (CH—CHA) site (47°12′36.8″ N, 8°24′37.6″ E, 393 m asl.) is a permanent temperate grassland located on a broad (around 16 km) valley bottom in the Canton of Zug, Switzerland. The mean vegetation height is kept at 10–30 cm through repeated mowing, and the leaf area index (LAI) was 1.5–2.5 m^2 m^{-2} during our field campaigns. The soil texture was 35.8% sand, 45.2% silt, and 19.0% clay (in percent by mass) in the 0–20 cm layer (Roth, 2006). The average annual

Table 1
Precipitation and temperature conditions in the dry-hot summers 2018 and 2019 as compared to the 2006–2017 averages according to our measurement at the CH-CHA site.

Environmental variables	2018	2019	2006–2017
Annual precipitation [mm]	870	1070	1167
Average annual temperature [°C]	11.2	10.4	9.9
Summer precipitation (June–September) [mm]	374	417	541
Average summer temperature (June–September) [°C]	19.1	18.6	17.5

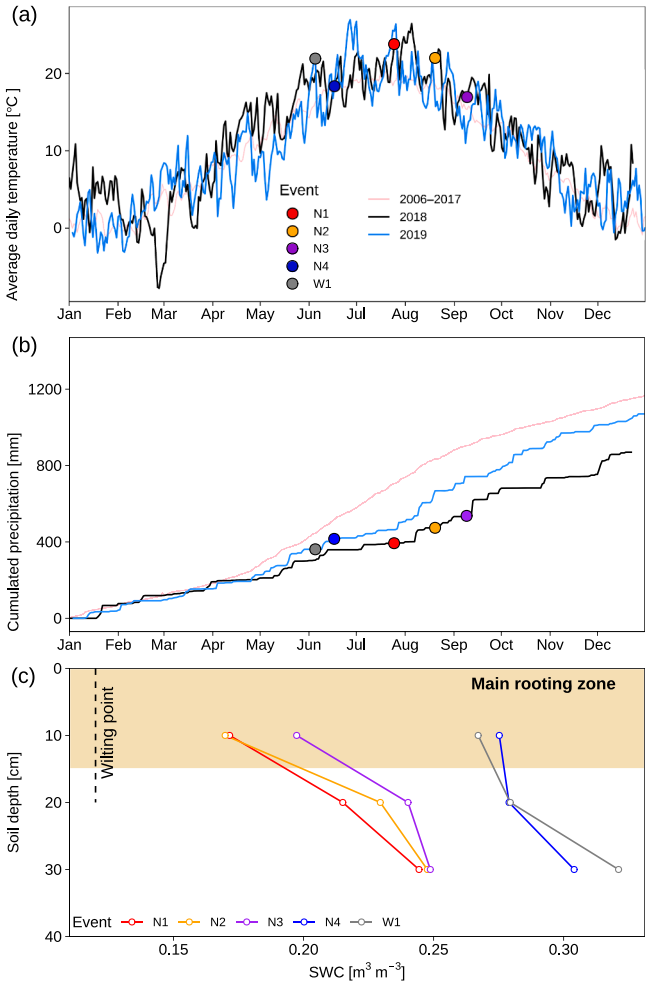

Fig. 1. Climatic conditions during dry-hot summers 2018 and 2019. (a) Average daily air temperature in 2018 and 2019 as compared to the average daily temperature for the years 2006–2017. Symbols indicate the corresponding average daily temperature during the five events, i.e., N1, N2, N3 events in summer 2018, and N4, N5 events in summer 2019 (N1–N4 events with non-rainfall water (NRW) inputs on the nights, and W1 without NRW inputs during the night). (b) Cumulated precipitation in 2018 and 2019 as compared to the averages of cumulated precipitation for the period 2006–2017. Symbols indicate the corresponding cumulated precipitation prior to the five events. (c) Volumetric soil water content (SWC) during the five events at the 10 cm, 20 cm, and 30 cm soil depths. The main rooting zone (0–15 cm) is shaded in orange (96% of the belowground dry biomass, Prechsl et al., 2015); the permanent wilting point (vertical black dashed line) for the top 20 cm soil was 12% calculated from the soil water potential of –1500 kPa following Saxton et al. (1986).

precipitation and temperature were 1167 mm, and 9.9 °C, respectively during years 2006–2017 (Table 1). As compared to the levels over 2006–2017, the year 2018 had 25% less annual precipitation and was 1.3 °C warmer, whereas the year 2019 saw 8% less precipitation, and was 0.5 °C warmer (Table 1).

Long-term eddy-covariance (EC) measurements of H_2O and CO_2 fluxes were carried out with a three-dimensional ultrasonic anemometer-thermometer (model R3–50, Gill Instruments, Solent, UK) and an open-path Infrared Gas Analyzer (IRGA, Li-7500, Li-Cor, Lincoln, NB, USA) installed at 2.4 m above ground level (agl). Air temperature (T_{a2m}, °C), relative humidity (RH_{2m},%; combined HydroClip S3 sensor, Rotronic AG, Bassersdorf, Switzerland), and long-wave outgoing (LW_{out}, W m^{-2}; CNR1, Kipp & Zonen B.V., Delft, The Netherlands) and incoming (LW_{in}) radiation were measured at 2 m agl. Precipitation was measured at 0.5 m agl with a heatable tipping bucket rain-gage with a standard 200 cm^2 orifice (model 15188H, Lamprecht meteo GmbH, Göttingen, Germany). Horizontal mean wind speed (u, m s^{-1}), air pressure (p, kPa), dewpoint temperature (T_{dew}, °C) and H_2O vapor concentrations were measured with this EC set-up, and data were processed with the EddyPro software (Fuchs et al., 2018; LI-COR, 2019) following established community guidelines (Aubinet et al., 2012). The evapotranspiration rate (ET in mm h^{-1}) was then computed from H_2O vapor fluxes (F_{H2O}, mmol m^{-2} s^{-1}) by (Stull 1988):

$$ET = F_{H_2O} \cdot M_{H_2O}, \quad (1)$$

where $M_{H2O} = 18$ g mol^{-1} is molar mass of H_2O. The daily ET was then calculated.

Canopy surface temperature (T_0, °C) was determined following Stefan–Boltzmann's law by (Stull, 1988):

$$T_0 = \sqrt[4]{\frac{LW_{out} - (1 - \varepsilon) \cdot LW_{in}}{\varepsilon \cdot \sigma}} - 273.15, \quad (2)$$

where ε is the emissivity, assuming 0.98 for wet canopy surfaces (T_{0w}), and 0.96 for dry canopy surfaces (T_{0d}) following López et al. (2012); $\sigma = 5.67 \cdot 10^{-8}$ W m^{-2} K^{-1} is the Stefan-Boltzmann constant (Stull, 1988).

Volumetric soil water content (SWC, m^3 m^{-3}; ML2x and ML3, Delta-T Devices Ltd., Cambridge, UK) was measured at 10, 20 and 30 cm soil depths. The permanent wilting-point for 0–20 cm soil was 0.12 m^3 m^{-3} (Fig. 1c), calculated from the soil water potential of –1500 kPa following Saxton et al. (1986). The main rooting zone, i.e., 96% of the belowground dry biomass was in the 0–15 cm topsoil layer (Prechsl et al., 2015).

2.2. Observation campaigns during NRW and windy events

The observation campaigns were carried out during five nights: three during summer 2018, on 25–26 July, 20–21 August, and 9–10 September (N1, N2 and N3, respectively; Table 2), and two during summer 2019, on 17–18 June (N4), and 5–6 July (W1, without NRW input; Table 2). As compared to summer precipitation (541 mm on average) and temperature (17.5 °C on average) during 2006–2017, the 2018 and 2019 summers had 31% and 23% less precipitation, and were 1.6 °C and 1.1 °C warmer, respectively (Fig. 1b). Accumulated precipitation until the beginning of each of the five events was 83 to 368 mm less than the corresponding levels over 2006–2017 (Fig. 1a). SWC for N1–N3 in 2018 was 0.17–0.25 m^3 m^{-3}, which was lower than the levels of 0.27–0.32 m^3 m^{-3} for N4 and W1 in 2019; the SWC never reached the estimated wilting point (0.12 m^3 m^{-3}) during the five events (Fig. 1c).

During the nights of N1–N4, condensation started when leaf temperature reached the dewpoint ($T_0 \leq T_{dew}$) (Fig. 2a). N1–N4 with NRW inputs were clear-sky and calm nights ($u = 0.3$ m s^{-1}; Fig. 2b) with high RH_{2m} of 62–100% (Fig. 2c), whereas the W1 night was windy ($u = 2.2$ m s^{-1}; Fig. 2b) with RH_{2m} of 31–75% (Fig. 2c). Daily ET was larger during the two 2019 summer events (3.9 mm d^{-1}; Fig. 2d) than during the three 2018 summer events (2.3–3.4 mm d^{-1}), which was consistent with the lower SWC in 2018 than in 2019 (Fig. 1c). All the times are reported as CET (UTC + 01:00).

Table 2
Set-up of five sampling campaigns (N1–N4 events with non-rainfall water (NRW) inputs on the nights, and W1 without NRW inputs on the night) during dry-hot summers 2018 and 2019. Numbers after "*n*=" stands for the replicates of water samples for isotope analyses, leaf relative water content (RWC), and leaf water potential (LWP). NRW represents non-rainfall water, root represents xylem water of root crown, and leaf represents leaf water. "n.a." means NRW samples were not available because of dry leaves at the corresponding sampling time. NRW, leaf, and root crown xylem samples were taken from randomly selected plants of three genera *Lolium, Taraxacum* and *Trifolium.*

Year	Date	Event	Sunset, sunrise [CET]	Weather condition	Time [CET]	Isotope samples				RWC	LWP
						NRW	Leaf	Root	Soil		
2018	25–26 Jul	N1	20:09, 04:58	Pre-sunset	19:00	n.a.	$n = 3$	$n = 3$	$n = 1$		$n = 3$
				NRW night	03:00	$n = 3$	$n = 3$	$n = 3$	$n = 1$		$n = 3$
	20–21 Aug	N2	19:29, 05:31	Pre-sunset	19:00	n.a.	$n = 3$	$n = 3$	$n = 1$	$n = 3$	$n = 3$
				NRW night	23:00	$n = 3$	$n = 3$	$n = 3$	$n = 1$		$n = 3$
				NRW night	01:00	$n = 3$	$n = 3$	$n = 3$	$n = 1$		$n = 3$
				NRW night	03:00	$n = 3$	$n = 3$	$n = 3$	$n = 1$	$n = 3$	$n = 3$
				NRW night	05:00	$n = 3$	$n = 3$	$n = 3$	$n = 1$		$n = 3$
	9–10 Sep	N3	18:51, 05:57	Pre-sunset	18:30	n.a.	$n = 3$	$n = 3$	$n = 3$		
				NRW night	05:00	$n = 3$	$n = 3$	$n = 3$	$n = 3$		
2019	17–18 Jun	N4	20:25, 04:30	Pre-sunset	20:00	n.a.	$n = 3$	$n = 3$	$n = 3$	$n = 3$	
				NRW night	00:00	$n = 3$	$n = 3$			$n = 3$	
				NRW night	03:00	$n = 3$	$n = 3$	$n = 3$	$n = 3$		
	5–6 Jun	W1	20:18, 04:32	Pre-sunset	20:00	n.a.	$n = 3$	$n = 3$	$n = 3$		$n = 3$
				Windy night	00:00	n.a.	$n = 3$	$n = 3$			
				Windy night	03:00	n.a.	$n = 3$	$n = 3$	$n = 3$		$n = 3$

2.2.1. Destructive sampling for measurements of the isotope composition

To measure the isotope composition of water in NRW droplets, bulk leaf, root crown xylem, and soil, the corresponding samples were taken starting around 1-h before sunset, followed by regular sampling throughout the night (Table 2). Considering leaf characteristics, three genera were selected in the grassland vegetation: *Lolium* (long-narrow leaves), *Taraxacum* (long-wide leaves) and *Trifolium* (short-wide leaves). To minimize disturbance of destructive sampling on the effect of NRW formation, NRW droplets, leaf and root crown xylem samples were taken from different plants of each given genus within the sampling area. NRW samples were taken in triplicate ($n = 3$) from each given genus by absorbing approximately 1.0 mL of NRW droplets on leaf surfaces with cotton balls (Wen et al., 2012). Each sample was taken from randomly selected plants of the given genus. Bulk leaf samples were taken in triplicate ($n = 3$) for each given genus after having softly removed water from the leaf surfaces with tissue paper (Wen et al., 2012); each sample included 2–12 leaves from randomly selected different plants (only one leaf per plant was collected) of the same genus. The isotope composition for the xylem water of root crown best reflects the water taken up by roots (Barnard et al., 2006). Therefore, root crown samples were taken in triplicate ($n = 3$) for each given genus after having removed the attached soil and debris (Prechsl et al., 2015); each sample included one to six root crowns from randomly selected different plants of the same genus. Soil cores were taken at 0–5 cm, 5–10 cm, 10–15 cm, 15–20 cm, and 20–40 cm soil depths. In the W1 event, 20–40 cm soil samples were not available due to an operational mistake. During N1 and N2, soil samples were taken as single cores ($n = 1$), whilst for N3, N4 and W1, soil samples were taken in triplicate ($n = 3$).

All samples were transferred immediately into glass tubes (Labco Exetainer® 12 ml Vial, Labco Ltd., High Wycombe, UK), sealed with caps and parafilm, and stored in a portable cooling box during the field campaign. Samples were then taken to the laboratory and stored at –19 °C before extracting the water using a cryogenic vacuum distillation system (Prechsl et al., 2015). The extracted water was measured with an isotope ratio mass spectrometer (IRMS DELTAplus XP; Thermo-Finnigan, Bremen, Germany) to obtain the isotope composition of the respective water samples. The isotope composition of hydrogen or oxygen in water is expressed in the delta notation $\delta = (R_{sample}/R_{standard} - 1)$ in per mil (‰), where R_{sample} and $R_{standard}$ are the molar ratios of either $^{2}H/^{1}H$ or $^{18}O/^{16}O$ for the sample and the standard (Vienna Standard Mean Ocean Water, VSMOW; IAEA, 2009), respectively. With this definition, $\delta^{18}O$ and $\delta^{2}H$ are expressed as per mil (‰) deviations from the standard. The measured uncertainties of $\delta^{18}O$ and $\delta^{2}H$ values using IRMS were ±0.34‰ and ±0.73‰, respectively. Here, we define $\delta^{18}O$ ($\delta^{2}H$) of NRW droplets, leaf water, root crown xylem water, and soil water as $\delta^{18}O_n$ ($\delta^{2}H_n$), $\delta^{18}O_L$ ($\delta^{2}H_L$), $\delta^{18}O_r$ ($\delta^{2}H_r$), and $\delta^{18}O_s$ ($\delta^{2}H_s$), respectively.

2.2.2. Isotope composition of atmospheric water vapor and its equilibrium liquid

The isotope composition of atmospheric water vapor ($\delta^{18}O_v$ and $\delta^{2}H_v$) was measured using a cavity ring-down laser spectrometer (L2130-i, Picarro Inc., Santa Clara, CA, USA) during N1, N2 and N3 events in 2018 (see details in Li et al., 2021 and Aemisegger et al., 2012), which was not available in 2019. Atmospheric air was pulled into the L2130-i cavity through a PTFE intake hose, and a PTFE-filter inlet (FS-15–100 and TF50, Solberg International Ltd., Itasca, IL, USA) fixed at 6 m agl. The instrument's response time in this setup was on the order of 10 s (Aemisegger et al., 2012). To correct for instrument drifts and to normalize the data to the international VSMOW-SLAP scale, the raw data were calibrated using a Standard Delivery Module (SDM; A0101, Picarro Inc., Santa Clara, CA, USA) by performing two-point calibrations every 12 h (Aemisegger et al., 2012; Thurnherr et al., 2020). The calibrated $\delta^{18}O_v$ and $\delta^{2}H_v$ data were averaged to 30 min intervals.

2.2.3. Leaf water potential (LWP) and leaf relative water content (RWC)

During the before-sunset and predawn periods of N1, N2 and W1, leaf water potential (LWP) for *Lolium, Taraxacum*, and *Trifolium* was measured in triplicate ($n = 3$) with a Scholander pressure chamber (Model 1505D, PMS Instruments Co., Albany, OR, USA). LWP was not available during N3 and N4.

To test whether leaves reached turgid leaf water content during NRW inputs, the leaf relative water content (RWC) was determined during pre-sunset and nighttime periods in N2 and N4 (Table 2) by triplicated ($n = 3$) sampling. The RWC was calculated as (Barrs and Weatherley, 1962):

$$RWC = (FW - DW)/(TW - DW), \quad (3)$$

where FW is the initial fresh weight of bulk leaves, TW is the full-turgor weight, and DW is the dry weight. FW was weighed after softly removing the attached droplets from bulk leaves with tissue paper. TW was weighed after floating the initial fresh leaf in distilled water for 3 h and softly removing the attached droplets with tissue paper (Fricke et al., 2004). DW was weighed after drying the bulk leaves at 60 °C for 24 h.

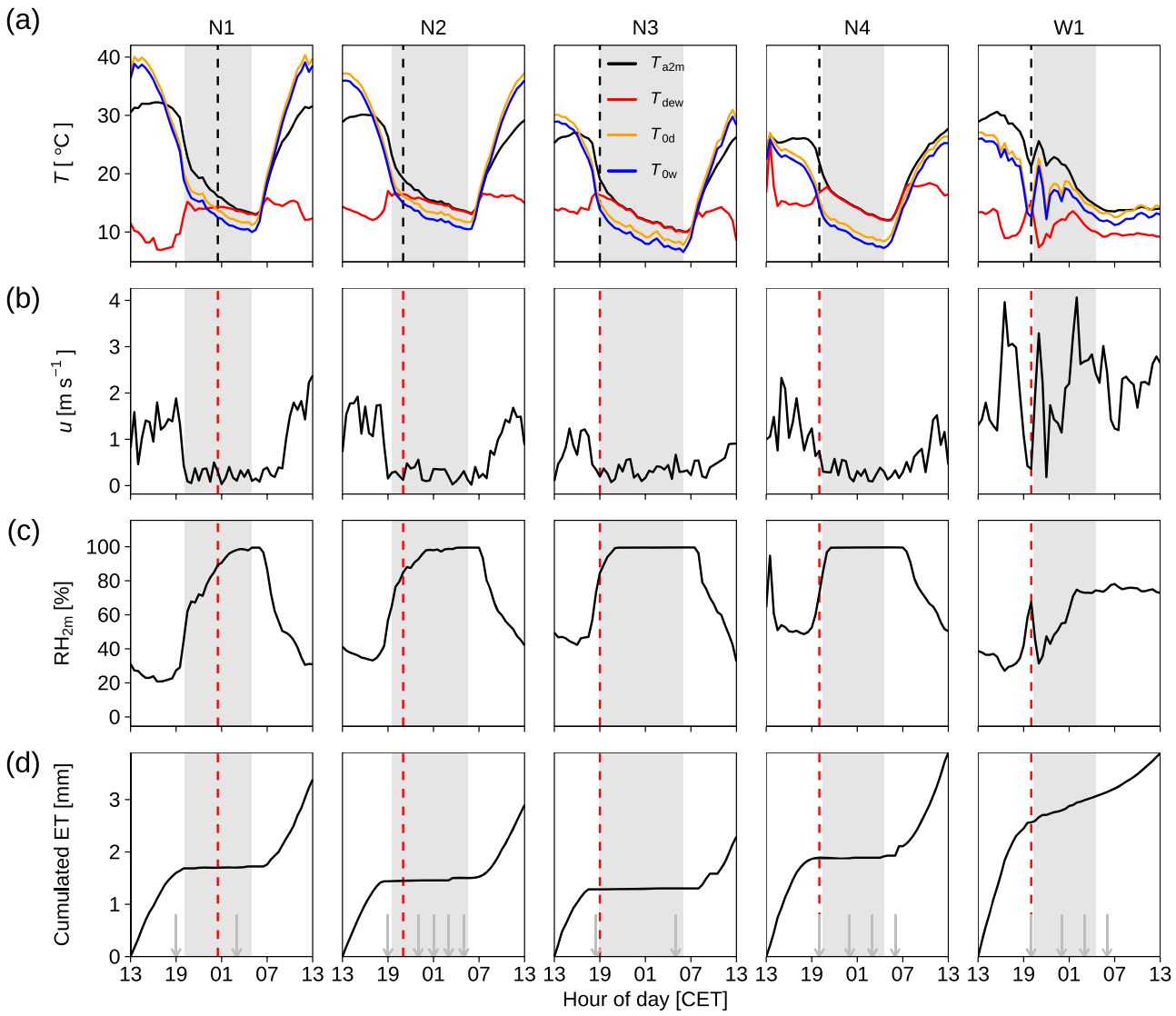

Fig. 2. Environmental variables during five sampling campaigns (N1–N4 events with non-rainfall water (NRW) inputs on the nights, and W1 without NRW inputs on the night): (a) air temperature (T_{a2m}), dew point temperature (T_{dew}) and canopy surface temperature under the assumptions of dry canopy surface (T_{0d}), and wet canopy surface (T_{0w}); (b) horizontal mean wind speed at 2 m agl. (u); (c) relative humidity (RH_{2m}) at 2 m agl.; (d) daily cumulated evapotranspiration (ET) amount. gray shaded areas indicate nighttime periods, and vertical red dashed lines show the timing of the first sign of condensation. gray vertical arrows in panel (d) indicate the sampling time.

2.3. Leaf temperature simulation

Leaf temperature (T_L) estimation strongly affects the simulation of total leaf conductance (g_L), hence we used different methods to estimate leaf temperature:

$(LT1) T_L = T_{0w};$

$(LT2) T_L = T_{0d};$

$(LT3) T_L = T_{0w} + T_{dif};$

$(LT4) T_L = T_{0d} + T_{dif};$

For the methods LT3 and LT4, T_{dif} is the temperature difference between species-specific leaf and the canopy surface. We note that a thermal image was taken on N4 night (at 04:11 on 18 June 2019, Fig. S1), but was used for N2 night adopting a regression of T_0 between N2 and N4 night values (see Fig. S2 for the regression). According to the thermal camera image taken on N4 night (Fig. S1), T_L of *Lolium, Taraxacum* and *Trifolium* on N4 night were 0.9 °C cooler, 0.1 °C warmer, and 0.3 °C warmer as compared to the canopy surface temperature, respectively. According to the regression of T_0 between N2 and N4 night, T_L of *Lolium* was 0.8 °C cooler, *Taraxacum* 0.1 °C warmer, and *Trifolium* 0.3 °C warmer on N2 night, as compared to canopy surface temperature, hence T_{dif} on N2 night was given –0.8, 0.1 and 0.3 °C for *Lolium, Taraxacum* and *Trifolium*, respectively. We assumed that T_{dif} was constant over N2 night for a specific species, but the actual T_{dif} could indeed be variable.

2.4. Equilibrium liquid of atmospheric water vapor

The isotope composition ($\delta^{18}O_{eq}$ and $\delta^{2}H_{eq}$) of the liquid in equilibrium with ambient water vapor under wet leaf surface temperature T_{0w} was calculated following Horita and Wesolowski (1994):

$$\delta_{eq} = \alpha_{eq} \cdot (10^3 + \delta_v) - 10^3, \quad (4)$$

where the equilibrium fractionation factor α_{eq} was expressed as:

$$\alpha_{eq} = \exp\left(0.35041\cdot\frac{10^6}{(T_0+273.15)^3} - 1.6664\cdot\frac{10^3}{(T_0+273.15)^2} + \frac{6.7123}{T_0+273.15} - \frac{7.685}{10^3}\right) \text{for } ^{18}O, \quad (5)$$

and

$$\alpha_{eq} = \exp\left(1.1588\cdot\frac{(T_0+273.15)^3}{10^9} - 1.6201\cdot\frac{(T_0+273.15)^2}{10^6} + 0.79484\cdot\frac{(T_0+273.15)}{10^3} - 0.16104 + 2.9992\cdot\frac{10^6}{(T_0+273.15)^3}\right) \text{for } ^{2}H. \quad (6)$$

We note that giving T_{0w}, T_{0d} or species-specific T_L for T_0 in Eqs. (5) and 6 induced <0.15‰ and <1.8‰ differences of the simulated $\delta^{18}O_{eq}$ and $\delta^{2}H_{eq}$, which was at the magnitude of IRMS measurement errors. Therefore, the wet or dry leaf surface assumptions had minor effect on the $\delta^{18}O_{eq}$ and $\delta^{2}H_{eq}$ simulations.

2.5. Simulating total leaf conductance based on an isotope mass balance

On the dew night during N2 event with NRW inputs, we computed total leaf conductance (g_L) based on the non-steady state leaf water enrichment model by Farquhar and Cernusak (2005):

$$g_L = \frac{\alpha_k \cdot \alpha_{eq}}{w_i \cdot (\Delta_{Ls} - \Delta_L)} \cdot \frac{1 - e^{-\wp}}{\wp} \cdot \frac{d(W \cdot \Delta_L)}{dt}, \quad (7)$$

where Δ_L is measured leaf water ^{18}O enrichment (at non-steady state) and Δ_{Ls} is the simulated leaf water enrichment at steady-state; W is leaf water concentration in mol m $^{-2}$ s $^{-1}$; w_i is the mole fraction of water vapor in the leaf intercellular spaces; t is time step; $\wp$ is Péclet number; α_k is the kinetic fractionation factor.

The Péclet number $\wp$ is calculated as:

$$\wp = \frac{\text{Advective transport rate}}{\text{Diffusive transport rate}} = \frac{E \cdot L}{C \cdot D}. \quad (8)$$

where L in m is the distance from the site of evaporation, $C = 5.55{\cdot}10^4$ mol m^{-3} is the concentration of water, and $D = 2.66{\cdot}10^{-9}$ m^2 s^{-1} is the diffusivity of H_2O in liquid water (Wang et al., 1998); E in mol m^{-2} s^{-1} is the evaporation rate.

During dew and radiation fog nights in this study, E was $\leq 10^{-4}$ mol m^{-2} s^{-1}, L was $\leq 10^{-2}$ m for *Lolium, Taraxacum*, and *Trifolium*, hence $\wp \rightarrow 0$ (<0.01). Therefore, the term $(1 - e^{-\wp})/\wp$ is close to unity (>0.99).

With the term $(1 - e^{-\wp})/\wp$ close to unity during NRW input nights, Eq. (7) was approximated as:

$$g_L \approx \frac{\alpha_k \cdot \alpha_{eq}}{w_i \cdot (\Delta_{Ls} - \Delta_L)} \cdot \frac{d(W \cdot \Delta_L)}{dt}. \quad (9)$$

The ^{18}O enrichment of water pool "x" was defined with respect to $\delta^{18}O_r$ (Cernusak et al., 2016) as:

$$\Delta_x = \frac{\delta^{18}O_x - \delta^{18}O_r}{1 + \delta^{18}O_r}, \quad (10)$$

where $\delta^{18}O_r$ is the average value over N2 night by species. $\delta^{18}O_L$ was measured at 19:00, 23:00, 01:00, 03:00, and 05:00 during N2, and the corresponding Δ_L was calculated; Δ_L at 21:00 was exponentially interpolated using the data at 19:00 and 23:00, hence 2-h interval of Δ_L was used for g_L simulation.

The values of W were calculated from our measured FW and DW, as well as specific leaf area (SLA: 0.0247, 0.0249, and 0.0203 m^2 g^{-1} for *Lolium, Taraxacum* and *Trifolium*, respectively, measured by Stohler, 2006) as:

$$W = \frac{(FW - DW)}{DW \cdot SLA \cdot 18g\ mol^{-1}}. \quad (11)$$

where FW and DW were measured at 19:00 and 03:00 during N2, and the corresponding W at 19:00 and 03:00 was calculated. W was interpolated into 2-h intervals following the same change trends as Δ_L. W at 05:00 was assumed the same as that at 03:00.

With the term $(1 - e^{-\wp})/\wp$ close to unity during NRW input nights, the simulated Δ_{Ls} following Farquhar and Lloyd (1993) is:

$$\Delta_{Ls} = \frac{\Delta_e \cdot (1 - e^{-\wp})}{\wp} \approx \Delta_e = (1 + \epsilon_{eq}) \cdot [1 + \epsilon_k + \frac{e_a}{e_i} \cdot (\Delta_v - \epsilon_k)] - 1, \quad (12)$$

where Δ_v is the ambient water vapor enrichment calculated from $\delta^{18}O_v$ using Eq. Eq. (10); Δ_e is the water enrichment at the evaporative site. The simulations of Δ_{Ls} were based on 30-min data, but only used the corresponding Δ_{Ls} values at the times of our simulations (i.e., at 19:00, 21:00, 23:00, 01:00, 03:00, and 05:00 during N2).

The kinetic fractionation factor ϵ_k in per mil (‰) was 28 ‰ for ^{18}O and 25 ‰ for ^{2}H (Lee et al., 2009) given the diffusivity ratio of D_{major}/D_{minor} (^{18}O) = 0.9723 and D_{major}/D_{minor} (^{2}H) = 0.9755 following Merlivat (1978).

The leaf internal vapor pressure (e_i, kPa) is (Stull, 1988):

$$e_i = 0.6112 \cdot \exp\left(\frac{17.67 \cdot T_0}{T_0 + 243.5}\right) \quad (13)$$

The value of w_i is thus calculated as:

$$w_i = \frac{e_i}{p}. \quad (14)$$

The atmospheric vapor pressure (e_a) is:

$$e_a = 0.6112 \cdot \exp\left(\frac{17.67 \cdot T_a}{T_a + 243.5}\right) \cdot RH_{2m}. \quad (15)$$

For the simulation of g_L using Eq. (9), the time interval was 2-h in this study. Previous research (Cernusak et al., 2002; Kahmen et al., 2009) recommended smaller time intervals pertinent to environmental stability (see temporal dynamics of corresponding RH_{2m}, T_a and $\delta^{18}O$ in Fig. S3). But the nighttime Δ_L variations were much smaller than the daytime Δ_L variations, which could induce unrealistic values of simulated g_L. According to our measurement during N2, 30-min changes of Δ_L (exponentially interpolated into 30-min) for ^{18}O was 0.2 ‰ on average, which was smaller than the measurement error of the IRMS

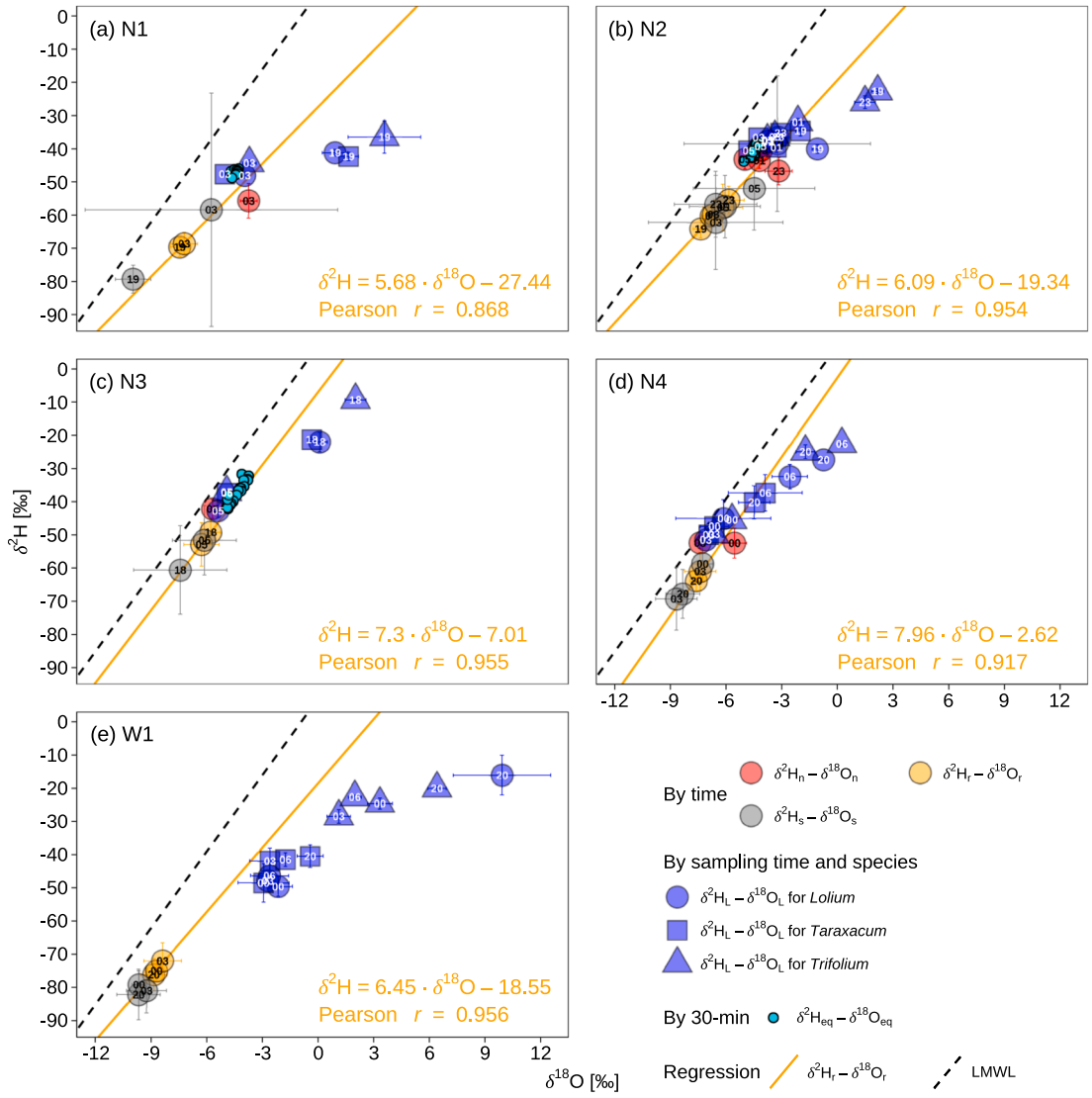

Fig. 3. Isotope composition for NRW droplets (δ^2H_n and $\delta^{18}O_n$) on foliage, xylem water of root crown (δ^2H_r and $\delta^{18}O_r$), soil water (δ^2H_s and $\delta^{18}O_s$) at 0–40 cm depth, and the liquid (δ^2H_{eq} and $\delta^{18}O_{eq}$) in equilibrium with atmospheric water vapor, and leaf water (δ^2H_l and $\delta^{18}O_l$) during five sampling campaigns (N1–N4 events with non-rainfall water (NRW) inputs on the nights, and W1 without NRW inputs on the night). Isotopes of NRW, root and soil were averaged by sampling time, isotopes of the liquid in equilibrium with atmospheric water vapor were shown with 30-min intervals, and leaf water isotopes were averaged by sampling time and species. The numbers within the symbols show the hour of day (CET) of the sampling. The error bars show the standard devation. The local meteoric water line (LMWL) for the isotope pairs of local precpitation follows Prechsl et al. (2014).

system. Thus, we used longer time (2-h) intervals for the simulation of g_L, but the 30-min interval simulation is shown in Table S2, and discussed in Section 4.3.

2.6. Air–leaf vapor exchange

The water vapor flux (D) between leaf and atmosphere is given by (Farquhar and Cernusak, 2005):

$$D = g_L \cdot (w_a - w_i), \quad (16)$$

where w_a is the mole fraction of water vapor in the atmospheric air calculated from e_a as:

$$w_a = \frac{e_a}{p}. \quad (17)$$

The unit of g_L from mol m^{-2} s^{-1} to m s^{-1} (written as G_L) was (Pearcy et al., 1989):

$$G_L[\text{m s}^{-1}] = \frac{g_L[\text{mol m}^{-2}\ \text{s}^{-1}]}{44.6} \cdot \left(\frac{T_a+273.15}{273.15}\right) \cdot \left(\frac{101.3}{p}\right)]. \quad (18)$$

Therefore, the air–leaf water vapor exchange rate (I_n) in mm s^{-1} was expressed as (Arkebauer, 2005):

$$I_n = 0.622 \cdot \rho \cdot G_L \cdot (w_a - w_i) \quad (19)$$

where ρ is the density of dry air given as 1.2 kg m^{-3} (Stull, 1988). Therefore, the air–leaf water exchange amount for the whole night was ΣI_n in mm $night^{-1}$.

Leaf boundary layer conductance (G_b in m s^{-1}) was estimated as:

$$G_b = 0.00662 \sqrt{\frac{u_{2m}}{L_L}}, \quad (20)$$

where L_L in m is the characteristic dimension of the leaf (i.e., leaf width, given 0.005, 0.05, and 0.02 m for *Lolium, Taraxacum* and *Trifolium*, respectively). Using Eq. (18), G_b in m s^{-1} was transformed into g_b (leaf

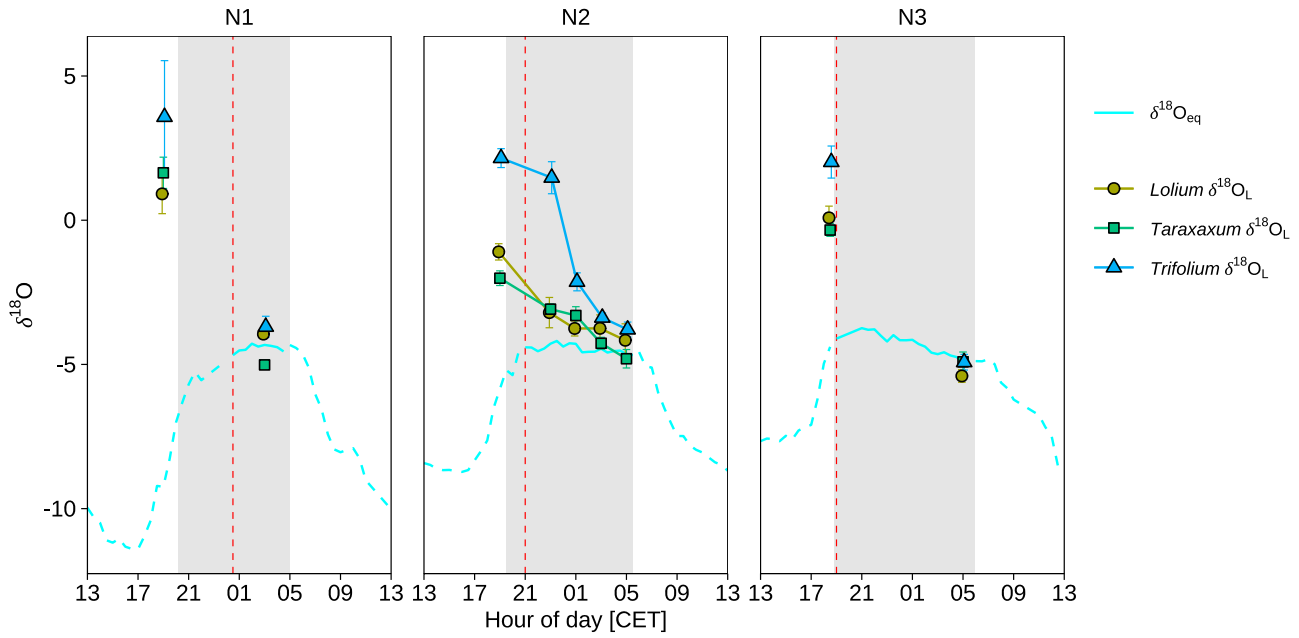

Fig. 4. Isotope composition of leaf water ($\delta^{18}O_L$) with respect to the isotopes ($\delta^{18}O_{eq}$) of the liquid in equilibrium with atmospheric water vapor during N1, N2, and N3 events with non-rainfall water inputs on the nights. The vertical red dashed lines indicate the start of condensation, and gray shaded area corresponds to nighttime periods.

boundary layer conductance) in mol m^{-2} s^{-1}.

Stomata conductance (g_s in mol m^{-2} s^{-1}) was estimated as (Pearcy et al., 1989):

$$g_s = \frac{1}{1/g_t - 1/g_b}. \quad (21)$$

We note that g_s using Eq. (21) was actually the sum of stomatal conductance, and cuticular conductance etc.

2.7. Stomatal size

Stomatal images of *Lolium* were taken using a digital microscope (AM7515MT8A Dino-Lite Edge, Dino-Lite Europe, Almere, The Netherlands) at around sunset before condensation started, and during leaf wetting by dew formation on 6–7 August 2020. The length and width of the stomata were measured using DinoCapture 2.0 software (Dino-Lite Europe, Almere, The Netherlands).

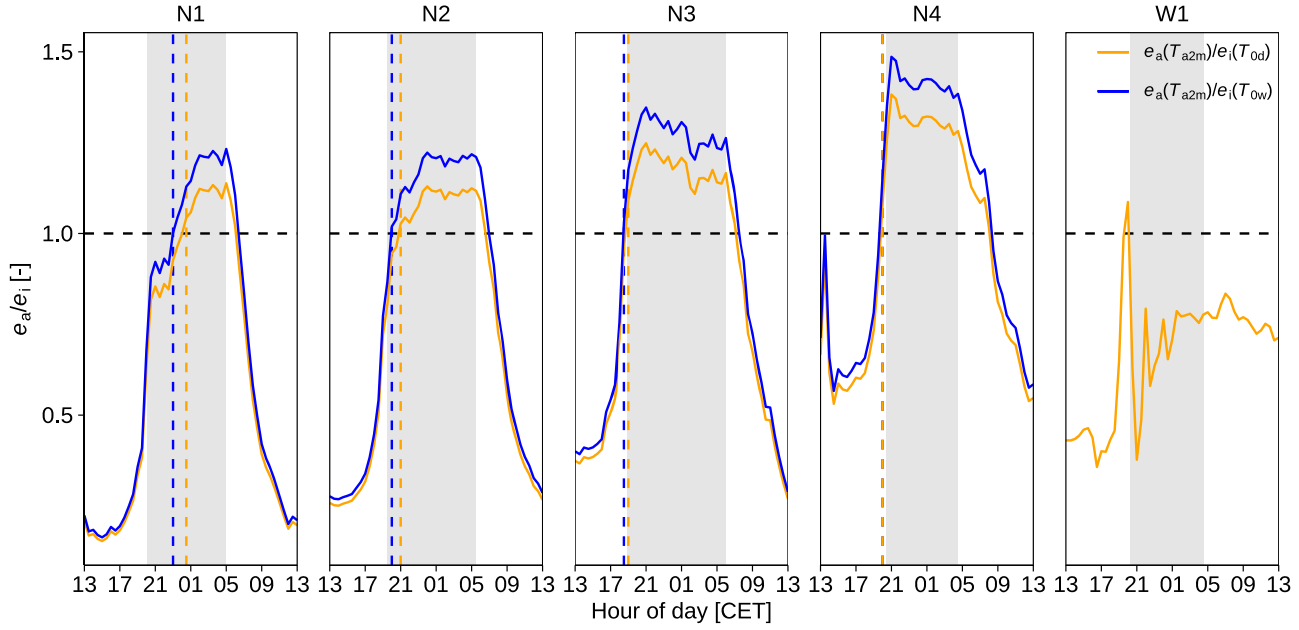

Fig. 5. Ratio of atmospheric vapor pressure (e_a), and vapor pressure within leaves (e_i) computed from dry (orange) and wet (blue) leaf surface temperatures during five sampling campaigns (N1–N4 events with non-rainfall water (NRW) inputs on the nights, and W1 without NRW inputs on the night). gray shaded areas indicate nighttime periods, and vertical orange and blue dashed lines show the turning point from $e_a/e_i<1$ to $e_a/e_i>1$.

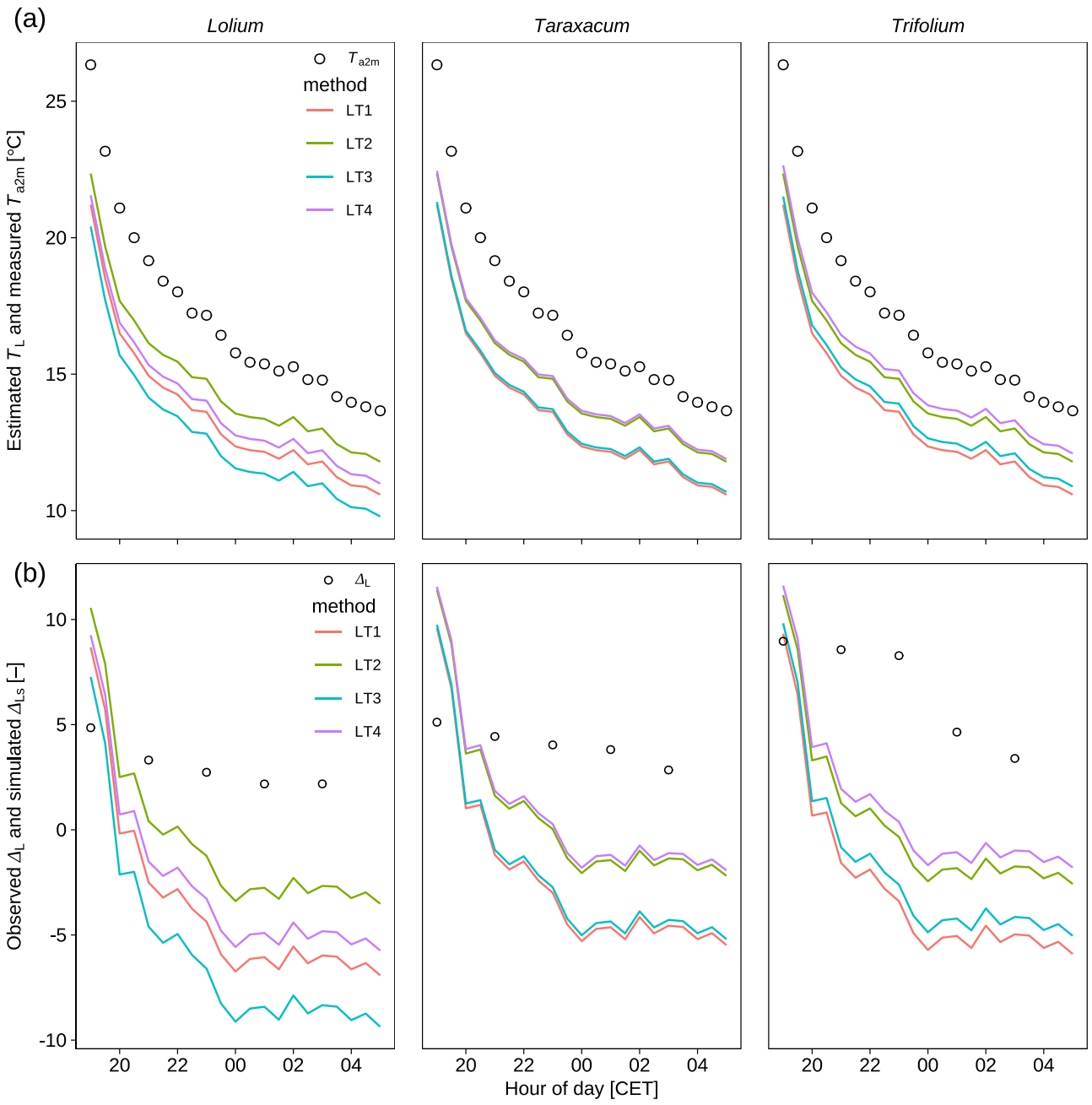

Fig. 6. Estimated leaf temperature (T_L) and simulated steady-state leaf water enrichment (Δ_{Ls}) under different methods of leaf temperature simulations (LT1-LT4) during N2 night with non-rainfall water (NRW) inputs: (LT1-LT2) Leaf temperature is assued as wet (T_{0w}) and dry (T_{0w}) canopy surface temperature. (LT3-LT4) Leaf temperature is assumed as $T_{dif} + T_{0w}$ (T_{0d}), where T_{dif} is the temperature difference between leaf and canopy surface by thermal imaging. (a) Estimated T_L using methods of LT1-LT4 as compared to atmospheric air temperature (T_{a2m}) at 2 m agl. (b) Simulated Δ_{Ls} as compared to observed leaf water enrichment (Δ_L).

2.8. Statistics and imaging

All statistical processing of the data was done with R version 4.0.4 (R Core Team, 2021). For the linear regression between δ^2H and $\delta^{18}O$, the orthogonal regression approach following Gat (1981) was used.

3. Results

3.1. Impact of NRW inputs on the leaf water isotope signal

We compared the δ^2H–$\delta^{18}O$ pairs of different water pools to distinguish between the main drivers of δ^2H_L–$\delta^{18}O_L$ variability. Soil water shows large variability in δ^2H_s and $\delta^{18}O_s$. δ^2H_r and $\delta^{18}O_r$ pairs for xylem water of root crown showed a correlation that agrees with that expected for unfractionated source water during all five events for both NRW and windy events (r: 0.868 to 0.956; Fig. 3). In contrast to soil water and xylem water of root crown, different environmental conditions strongly influenced leaf water dynamics, hence δ^2H_L–$\delta^{18}O_L$ of leaf water showed a much stronger variability (Fig. 3; Fig. S4). Before sunset of all the five events, as shown at 19:00 of N1 and N2, 18:30 of N3, as well as 20:00 of N4 and W1, all δ^2H_L–$\delta^{18}O_L$ pairs fell on the right-hand side of their corresponding δ^2H_r–$\delta^{18}O_r$ regression (Fig. 3). This was due to the evaporative process during daytime that caused an enrichment of leaf $\delta^{18}O_L$ and δ^2H_L. However, with the occurrence of nighttime NRW inputs as shown at 03:00 of N1, 01:00, 03:00 and 05:00 of N2, 05:00 of N3, as well as 00:00 and 03:00 of N4, δ^2H_L–$\delta^{18}O_L$ pairs fell on the left-hand side

Table 3
Simulated total leaf conductance (g_L, mmol m^{-2} s^{-1}, average±standard deviations; the values at each time step are shown in Table S1), leaf boundary layer condutance (g_b), stomatal condutance (g_s), and air–leaf water exchange amount (ΣI_n in mm $night^{-1}$, where I_n in mm s^{-1} is air–leaf vapor exchange rate) under the different assumptions of leaf temperature (T_L): (LT1 and LT2) Leaf temperature is assued as wet (T_{0w}) and dry (T_{0w}) canopy surface temperature. (LT3 and LT4) Leaf temperature is assumed as T_{dif} + T_{0w} (T_{0d}), where T_{dif} is the temperature difference between leaf and canopy surface by thermal camera imaging. NRW-input (non-rainfall water input) was 0.26 mm $night^{-1}$ on N2 night following our previous study in Li et al. (2021).

Variable	Species	(LT1) g_L (T_L = T_{0w})	(LT2) g_L (T_L = T_{0d})	(LT3) g_L ($T_L = T_{dif}$ +T_{0w})	(LT4) g_L ($T_L = T_{dif}$ +T_{0d})
g_L [mmol m^{-2} s^{-1}]	*Lolium*	31±21	53±37	25±16	42±25
	Taraxacum	21±14	34±23	21±15	36±24
	Trifolium	39±49	56±68	42±53	62±76
g_b [mmol m^{-2} s^{-1}]	*Lolium*	1842±11	1842±11	1842±11	1842±11
	Taraxacum	582±6	582±6	582±6	582±6
	Trifolium	921±8	921±8	921±8	921±8
g_s [mmol m^{-2} s^{-1}]	*Lolium*	32	54	25	43
	Taraxacum	21	36	22	38
	Trifolium	41	59	44	67
ΣI_n [mm $night^{-1}$]	*Lolium*	0.048	0.045	0.049	0.055
	Taraxacum	0.032	0.029	0.031	0.028
	Trifolium	0.064	0.047	0.057	0.041
ΣI_n / (NRW-input)	*Lolium*	18%	17%	19%	21%
	Taraxacum	12%	11%	12%	11%
	Trifolium	25%	18%	22%	16%

of δ^2H_r–$\delta^{18}O_r$ regression. This suggested that the evaporation-derived enrichment signal was diluted by an additional water source besides water via root uptake. Particularly, in the first hours of condensation as shown at 23:00 of N2, δ^2H_L–$\delta^{18}O_L$ varied among species, with *Trifolium* δ^2H_L–$\delta^{18}O_L$ falling on the right-hand side of δ^2H_r–$\delta^{18}O_r$ regression as in the pre-sunset period, but *Lolium* and *Taraxacum* δ^2H_L–$\delta^{18}O_L$ moving towards the left-hand side (Fig. 3). This suggests a species-specific effect of dew and fog processes on the leaf water isotopes of different plant species.

After a NRW night as shown at 06:00 of N4, δ^2H_L–$\delta^{18}O_L$ pairs moved back to the right-hand side of the corresponding δ^2H_r–$\delta^{18}O_r$ regression line (Fig. 3), indicating that the evaporative process becomes again the dominant factor in affecting the leaf water isotopes. In contrast to the NRW nights, during the windy night without NRW inputs as shown at 00:00, 03:00, and 06:00 of W1 event, δ^2H_L–$\delta^{18}O_L$ always fell on the right-hand side of the corresponding δ^2H_r–$\delta^{18}O_r$ regression (Fig. 3), suggesting that water via root water uptake (RWU) was isotopically enriched in leaf water (heavy isotopologues) due to both daytime and nighttime evaporation. Especially, during the windy night in W1, $\delta^{18}O_L$ of *Trifolium* was 3.9‰ higher than the values of *Lolium* and *Taraxacum* (Fig. 3; Fig. S4), suggesting stronger evaporation for the leaf water of *Trifolium*, or a slower uptake of isotopically depleted water (heavy isotopologues) via root and/or leaf of *Trifolium*.

Under unsaturated conditions (RH_{2m}<100%; Fig. 2c) as shown at 03:00 of N1, δ^2H_L–$\delta^{18}O_L$ pairs deviated from δ^2H_n–$\delta^{18}O_n$ pairs on foliage, but were close to δ^2H_{eq}–$\delta^{18}O_{eq}$ pairs for equilibrium liquid of atmospheric water vapor (Fig. 3). In N2, leaf water of *Lolium* and *Taraxacum* equilibrated with atmospheric water vapor after 3.5 h (21:30 to 01:00; Fig. 4) of NRW exposure, but *Trifolium* roughly equilibrated with atmospheric water vapor after 5.5 h of NRW exposure (21:30 to 03:00; Fig. 4).In the first hours of condensation (i.e., 23:00 in N2), and during the windy W1 night, leaf water of *Trifolium* showed a more enriched isotope signal than that of *Lolium* and *Taraxacum* (Figs. 3, 4 and S4). This can be induced by stronger evaporative enrichment of *Trifolium* during daytime periods. More enriched leaf water of *Trifolium* before sunset also explains their slower equilibration with atmospheric water vapor during N2 event (Fig. 4) as compared to other species.

3.2. Effect of NRW inputs on the air–leaf vapor exchange and leaf water status

The vapor pressure gradient between leaf and atmosphere indicates the net flux direction of air–leaf water vapor exchange, with $e_a/e_i < 1$ (Fig. 5) when leaf internal vapor pressure is larger than ambient vapor pressure as seen during the daytime of N1–N4, and during the entire W1 period, when the net water vapor flux was directed from the leaf to the atmosphere under RH_{2m} < 67% (Fig. 2c), indicating vapor loss from the leaf. Whereas with $e_a/e_i(T_{0d}) > 1$ after 00:30 of N1, 21:30 of N2, 19:00 of N3, and 20:00 of N4 (Fig. 5), the net water vapor flux was directed from the atmosphere to the leaf under RH_{2m} in the ranges of 67–100% (Fig. 2c). As compared to dry leaf surfaces, leaf wetting resulted in 1.5 °C lower leaf temperature compared to a dry leaf (Fig. 2a), hence the turning point from $e_a/e_i < 1$ to $e_a/e_i > 1$ occurred 0.5–1.0 h earlier in N1–N3 for a wet leaf as compared to dry leaf conditions (Fig. 5).

The estimation of leaf temperature and the corresponding simulation of leaf water isotope enrichment varied under different methods of LT1-LT4 (Fig. 6). Total leaf conductance simulations using non-steady state leaf water enrichment model were affected by the methods of leaf temperature estimates. Using the different estimates of leaf temperatures (LT1-LT4), the simulated g_L ranged from 25±16 to 53±37 mmol m^{-2} s^{-1} for *Lolium*, from 21±14 to 36±24 mmol m^{-2} s^{-1} for *Taraxacum*, and from 39±49 to 62±76 mmol m^{-2} s^{-1} for *Trifolium* (Table 3). *Trifolium* had the highest g_L, and *Taraxacum* had the lowest g_L among the three species. The leaf boundary layer conductance (g_b) was 1842±11, 582±6, and 921±8 mmol m^{-2} s^{-1} (Table 3) for *Lolium, Taraxacum*, and *Trifolium*, respectively (Table 3). Stomatal conductance (g_s) using LT1-LT4 simulations was thus 25–54, 21–38, and 41–67 mmol m^{-2} s^{-1} for *Lolium, Taraxacum*, and *Trifolium*, respectively (Table 3).

Using the averages of g_L under each method of LT1-LT4, the respective air–leaf water exchange amount for *Lolium, Taraxacum*, and *Trifolium* was 0.048–0.055 mm $night^{-1}$, 0.028–0.032 mm $night^{-1}$, and 0.041–0.064 mm $night^{-1}$, respectively (Table 3). Furthermore, our previous study in Li et al. (2021) estimated that NRW input was 0.26 mm $night^{-1}$ during N2 night. Therefore, the respective air–leaf water exchange amount for *Lolium, Taraxacum*, and *Trifolium* was 17–21%, 11–12%, and 16–25% of the total NRW input during N2 night (Table 3).

Besides the air–leaf water exchange, leaf water status is also affected by RWU, which is driven by the water potential gradient between soil and leaf. With SWC above the wilting point (Fig. 1c), soil water potential was always higher than the LWP of measured plants (Fig. 7a). The soil water potential exceeded –0.3 MPa during N1 and N2, and was even higher than –0.1 MPa during W1 (Fig. 7a). The predawn LWP was generally higher ($p < 0.05$) for NRW events (N1 and N2; –0.3 ± 0.3 MPa) than the windy event (W1; –0.7 ± 0.3 MPa; Fig. 7a). For both NRW events (N1 and N2) and windy event (W1), LWP generally increased from before sunset to predawn periods (Fig. 7a). Especially, during N1 and N2, the Taraxacum LWP remained at higher levels of –0.3 ± 0.3 MPa as compared to the lower levels of LWP during windy W1 event (–0.7 ± 0.3 MPa; Fig. 7a). During N2 and N4, with NRW inputs, we observed an increase of RWC from before-sunset to predawn periods (Fig. 7b). At N2 predawn, leaf did not reach full turgor (Fig. 7b). At 00:00 of N4, all three genera reached their fully turgid leaf water content (Fig. 7b).

4. Discussion

4.1. Impact of NRW inputs on the leaf water isotope signal

According to our intensive sampling during N2 night, the leaf water isotopes reached equilibration with atmospheric air after 3.5–5.5 h of NRW exposure (Fig. 4). As compared to *Lolium* and *Taraxacum*, the isotope signal of *Trifolium* leaf water needed longer time to equilibrate with atmospheric water vapor (Fig. 4), which we attributed to their more enriched leaf water status during daytime as indicated by higher

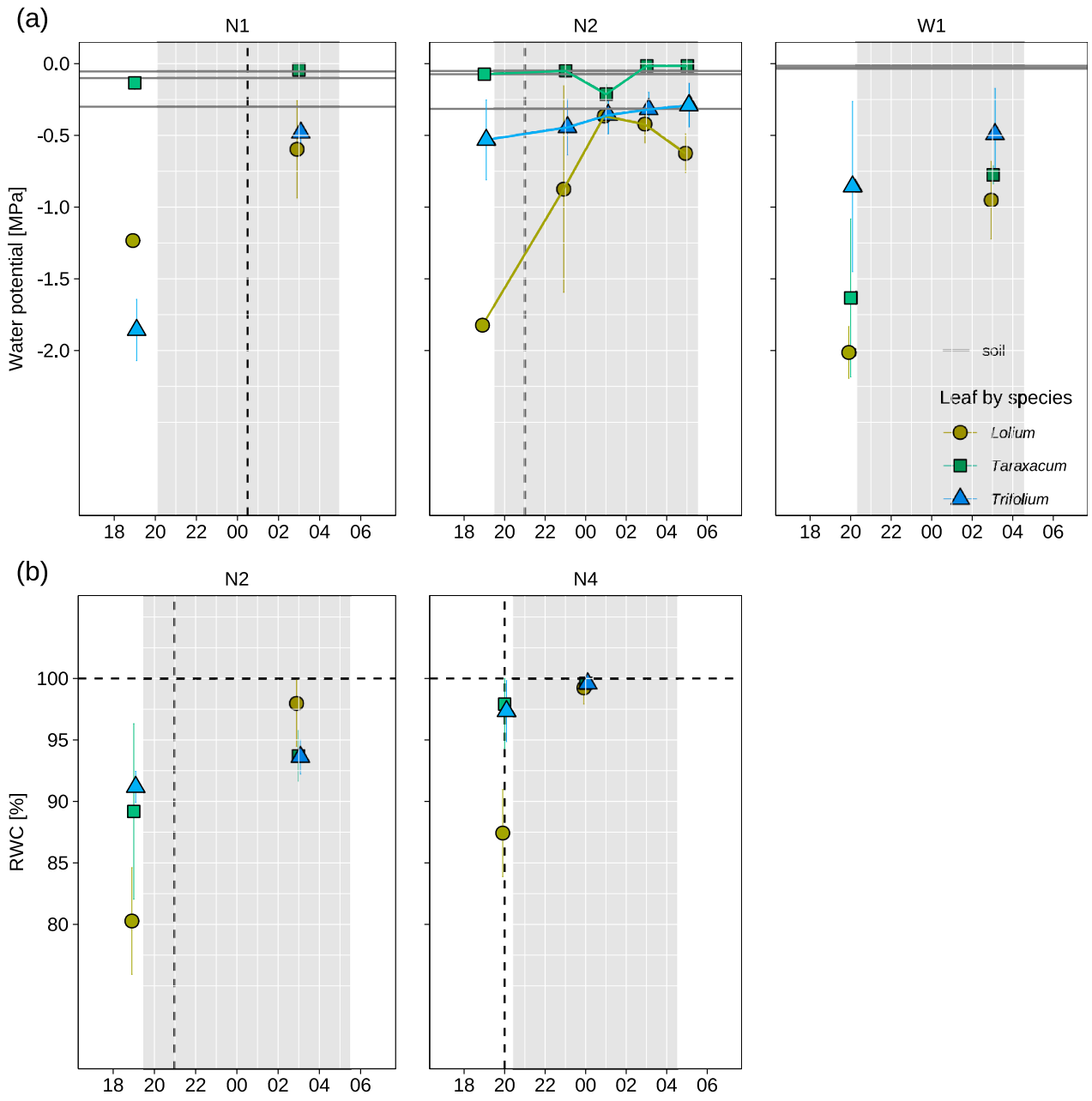

Fig. 7. Leaf water status: (a) leaf water potentials for three genera and soil water potential during N1, N2 and W1 events. (b) Leaf relative water content (RWC) during N2 and N4 events. Non-rainfall water (NRW) inputs occurred on the nights of N1, N2 and N4, whilst W1 night was windy without NRW inputs. gray shaded areas indicate nighttime periods, and vertical red dashed lines show the timing of the first sign of condensation.

$\delta^{18}O_L$ of *Trifolium* before sunset (Fig. 4).

Previous studies adding isotopically depleted or enriched water in chamber experiments reported that isotopic equilibration between leaf and the surrounding atmospheric water vapor was reached after around 5 h of exposure in simulated fog during daytime (Lehmann et al., 2018; Table 4), and after around 48 h of exposure in simulated dew in darkness (Kim and Lee, 2011; Table 4). The slower equilibration in these chamber experiments might be due to wall effects in combination with the continuous feeding of isotopically depleted water vapor from a mist generator (e.g., Lehmann et al., 2018) or a bubbler (e.g., Kim and Lee, 2011) into the chamber where plants were positioned. Thus, an equilibrium between leaf and water vapor could not be reached until the equilibrium between chamber water vapor and mist/bubbler water was achieved. Furthermore, grasses experience a faster isotope signal transfer from the surrounding atmosphere into leaf water compared to trees and shrubs, probably due to their small leaf water content, leaf thickness (Lehmann et al., 2020), and the presence of stomata on both sides of the leaves instead of only on the abaxial side. In our study, we only showed situations with dew or radiation fog occurrences when local water cycling was dominant (Kaseke et al., 2017; Li et al., 2021). Slower equilibrium can be expected with the occurrence of advection fog in natural conditions, during which the atmospheric water vapor isotopes can vary depending on the isotope signal and water vapor mixing ratio of the remote vapor source (Kaseke et al., 2017). Furthermore, the vegetation cover studied in this study was composed of short (< 30 cm) grasses and forbs with low LAI (≤ 2.5 m^2 m^{-2}; Section 2.1). Hence, the vertical variability of NRW inputs on leaf water isotopes was not as substantial as in higher (1 m) and/or more dense vegetation (LAI: 8 m^2 m^{-2}) as reported in Welp et al. (2008). Their leaf isotope signal in the upper-canopy with leaf wetting was in equilibrium with atmospheric

Table 4
Comparison of studies on air–leaf isotope exchange in chamber or laboratory experiments with this study.

Study	Method of NRW modification	Treated plant compartments	Air–leaf equilibrium
Kim and Lee (2011): chamber	Plant chamber was fed with water vapor generated by a bubbler filled with water of known isotope ratios at an airflow rate of 3.5 L min^{-1} (water vapor $\delta^{18}O$: –21.4‰ to –14.7‰)	Bulk plants	Almost reached after 48 h
Goldsmith et al. (2017): laboratory	Fog was generated using an ultrasonic fog machine and supplemented by periodic physical spraying for 1 h (fog $\delta^{18}O$: –50‰)	Bulk leaf after sealing the petiole	Not reached after 1 h
Lehmann et al. (2018): chamber	Fog was produced in a tent by ultrasonic mist generators placed in buckets of ^{18}O-depleted water. Fans were used to facilitate distribution of humid air throughout the tent (water vapor $\delta^{18}O$: –200‰)	Plant pots with soil covered by aluminum foil	Almost reached after 5 h
Gerlein-Safdi et al. (2018): laboratory	Adaxial side of treated leaf was misted with isotopeally labeled water ($\delta^{18}O = 8.8‰$) every half hour	Bulk leaf	No info given
This study: field conditions	Ambient conditions	Natural grassland	Reached after 3.5–5.5 h

Table 5
The stomatal sizes of *Lolium* at pre-sunset and predawn during a non-rainfall water input event on 6–7 August 2020. Means ± standard deviation (SD) is also given. Different letters indicate statistically significant differences ($p < 0.05$, Tukey's test) for the comparison between pre-sunset values with corresponding predawn values.

Time and condition	Stoma No.	Width (μm)	Length (μm)	Width/Length (μm)
19:35 CET pre-sunset dry leaf adaxial	1	9.3	33.0	0.28
	2	9.7	25.7	0.38
	3	11.1	32.8	0.34
	4	10.9	30.8	0.36
	5	10.1	32.0	0.32
	mean ± SD	10.2 ± 0.8[a]	30.9 ± 3.0[a]	0.33±0.04[a]
5:11 CET predawn wet leaf adaxial	1	13.7	28.9	0.48
	2	11.6	27.9	0.42
	3	10.3	26.9	0.38
	4	12.2	31.2	0.39
	5	11.7	31.1	0.38
	6	10.7	30.9	0.35
	7	10.3	35.8	0.29
	mean ± SD	11.9 ± 1.2[a]	29.2 ± 1.9[a]	0.41±0.04[a]

water vapor, whilst the lower-canopy leaves with dry surfaces showed a more enriched isotope composition and higher leaf temperatures than the upper-canopy leaves.

4.2. Effect of NRW inputs on the air–leaf water exchange and leaf water status

Radiative cooling, and leaf wetting by NRW droplets had a substantial effect on the air–leaf water exchange. Pre-NRW and during-NRW radiative cooling caused leaf surfaces to be cooler than the atmosphere, and thus switched the net flux direction of leaf–air vapor exchange (since 00:30 of N1, 21:30 of N2, 19:00 of N3, and 20:00 of N4; Fig. 5). Leaf wetting by NRW droplets alters the air–leaf vapor exchange in the first hours of NRW inputs. The dry canopy surface and wet canopy surface assumptions showed that the wet canopy surface was 1.5 °C cooler than the dry canopy surface due to the stronger radiative cooling induced by increasing emissivity via canopy wetting (López et al., 2012). This magnitude of temperature difference has a minor effect on the temperature-dependent equilibrium fractionation factor (0.1‰ difference for $\delta^{18}O$) but can switch the direction of air–leaf net vapor exchange in the first hours of condensation, i.e., bringing forward the switch of air–leaf net vapor exchange flux direction by 0.5–1.0 h (Fig. 5).

We applied the non-steady state leaf water enrichment model by Farquhar and Cernusak (2005) into the natural conditions with NRW inputs to estimate leaf conductance and thus focus primarily on the role of the thermal gradient and nocturnal stomatal behavior on air–leaf water exchange. Depending on the air–leaf thermal gradient, the averages of simulated stomatal conductance (g_s) using LT1-LT4 methods ranged from 21 to 67 mmol m^{-2} s^{-1} (Table 3), which was in the range of nocturnal g_s (26–142 mmol m^{-2} s^{-1}) for C_3 grasses reported by Ogle et al. (2012). Bollig and Feller (2014) reported that under drought treatment at the CH—CHA site as in this study, the respective daytime g_s of *Lolium* and *Trifolium* was 198±61 and 391±163 mmol m^{-2} s^{-1}. Therefore, night/day g_s ratio in this study was 10–27%, at the lower threshold of the night/day g_s ratio (34–73%) for C_3 grasses reported by Ogle et al. (2012). Moreover, as compared to the stomata size of the dry leaf shortly before sunset (with a stomatal conductance of 78–118 mmol m^{-2} s^{-1}, data not shown), the wet leaf during dew night had similar stomata size (Table 5; Fig. S5), suggesting that g_s during NRW input nights could have similar levels of g_s as during the short period before sunset. The among-species variability of leaf conductance can be primarily due to species-specific biophysical controls. The higher nocturnal stomatal conductance (g_s) of *Trifolium* (41–67 mmol m^{-2} s^{-1} using LT1-LT4 methods, Table 3) also corresponded to its higher daytime g_s (391 mmol m^{-2} s^{-1}, Bollig and Feller (2014)) as compared to *Lolium* (nighttime 25–54 mmol m^{-2} s^{-1}, Table 3; daytime 198 mmol m^{-2} s^{-1}, Bollig and Feller (2014)). Furthermore, the higher total leaf conductance (g_L) of *Trifolium* might be related to the trichomes on their leaf surfaces, because the scars of trichome shedding can increase total leaf conductance (Fernandez et al., 2014). Moreover, the waxy surfaces of *Taraxacum* might induce their smaller leaf conductance as compared to *Lolium* and *Trifolium*, and thus *Taraxacum* could always keep higher LWP from before-sunset until sunrise as shown during N1 and N2 events (Fig. 7a).

We assumed saturated leaf internal water vapor, but leaf internal vapor pressure is thought to be unsaturated for drought-stressed plants (Vesala et al., 2017; Cernusak et al., 2018; Wong et al., 2022). Under the assumption of unsaturated leaf internal vapor, smaller leaf internal vapor pressure can be expected by adding a relative-humidity parameter lower than unity in Eq. (13), and thus larger air–leaf vapor pressure gradient can be expected as compared to the saturated leaf internal conditions. As compared to atmospheric air temperature, both leaf surfaces and sub-stomatal cavity environment were cooler with dew and radiation fog occurrences in this study, hence condensation was expected to occur on both leaf surfaces and mesophyll cells within sub-stomatal cavities (Vesala et al., 2017). It is hard to distinguish the condensation occurring on leaf surfaces from the condensation occurring within sub-stomatal cavities, but NRW droplets condensing on the mesophyll cells within the substomatal cavities would be easier to be taken up by leaf cells as compared to the droplets on leaf surfaces. Uptake of liquid NRW water by the leaf needs to overcome high surface tension associated with the geometry of the stomata to enter leaves (Schonherr and Bukovac, 1972; Kim and Lee, 2011).

We found a generally higher predawn LWP for NRW events as compared to the windy predawn LWP (Fig. 7b). Soil water potential

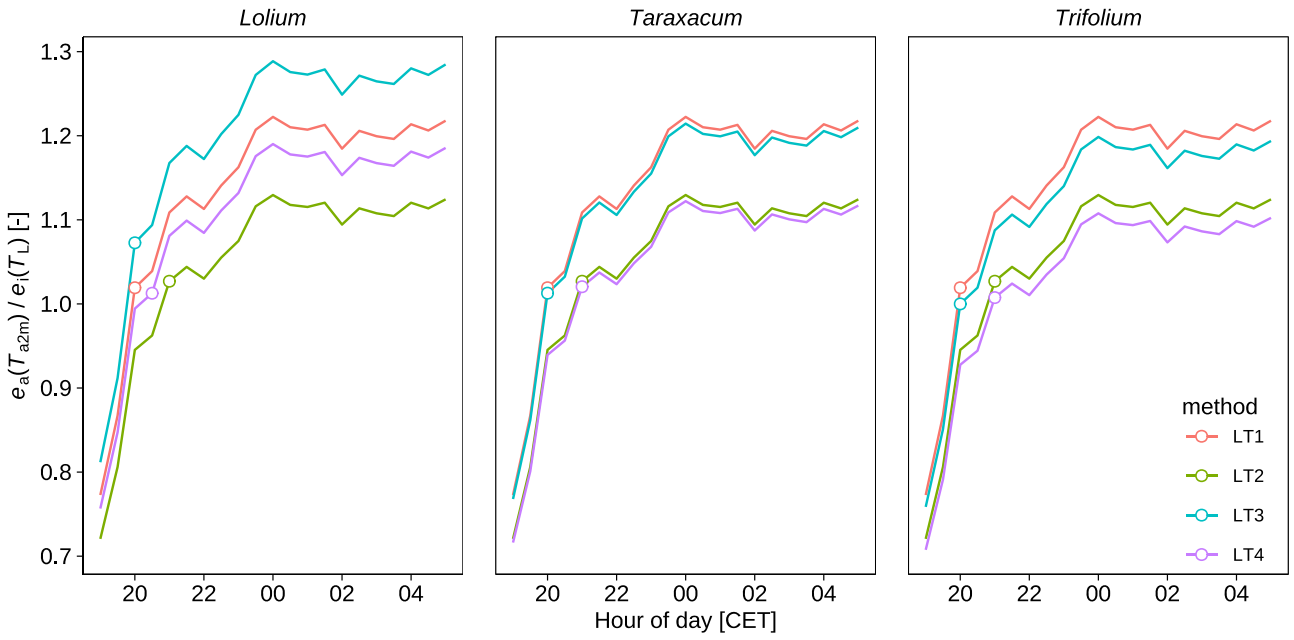

Fig. 8. Ratio of atmospheric vapor pressure (e_a), and vapor pressure within leaves (e_i) computed under different methods of leaf temperature simulations (LT1-LT4) during N2 night with non-rainfall water (NRW) inputs: (LT1-LT2) Leaf temperature is assued as wet (T_{0w}) and dry (T_{0w}) canopy surface temperature. (LT3-LT4) Leaf temperature is assumed as $T_{dif} + T_{0w}$ (T_{0d}), where T_{dif} is the temperature difference between leaf and canopy surface by thermal imaging.

during the four NRW events was still higher than LWP (Fig. 7a), despite the dry and hot conditions during summers of 2018 and 2019 (Fig. 1). Consequently, RWU might not be zero during NRW inputs when SWC is above the wilting point (Fig. 1c). *In-situ* experiments under extremely dry soil conditions would help to distinguish whether the observed leaf water status improvement was due to root uptake or foliar uptake, and whether stomata would still be open during the night with NRW inputs and soil water content below the wilting point.

4.3. Uncertainty of leaf temperature and conductance simulations

We used the methods of LT1-LT4 to estimate leaf temperature. LT1 and LT2 methods assumed species-indifferent leaf temperatures as canopy surface temperature, whilst LT3 and LT4 considered the among-species difference of leaf temperature using thermal imaging. LT1 and LT3 assumed wet leaf or canopy surfaces, whilst LT2 and LT4 assumed dry leaf or canopy surfaces. Considering among-species difference of leaf temperature (LT3 and LT4) induced up to 20% difference of g_L and 23% difference of air–leaf water exchange amount (ΣI_n) as compared to the methods assuming species-indifferent leaf temperatures (LT1 and LT2). The methods with wet surface assumptions (LT1 and LT3) induced up to 71% difference of g_L and 40% difference of ΣI_n, as compared to methods of dry surface assumptions (LT2 and LT4).

We also estimated leaf temperature using R-package "tealeaves" (Muir, 2019), which is based on the steady-state leaf energy budget. However, based on this estimation of leaf temperature, we simulated unrealistic values of g_L using isotope model (> 1000 or < 0 mmol m^{-2} s^{-1}, see Table S1). Unrealistic estimations of g_L using this method were caused by the fact that simulated steady-state Δ_{Ls} was very close to measured Δ_L (Fig. S6a), i.e., the term $1/(\Delta_{Ls} - \Delta_L)$ in Eq. (9) approached infinity ($-\infty$ or ∞), and thus unrealistic g_L was solved. The estimated T_L using "tealeaves"-package was close to air temperature (Fig. S6b). As a result, atmospheric vapor pressure was always lower than leaf internal vapor pressure (i.e., $e_a/e_i < 1$, Fig. S6c), because of leaf internal saturation vs unsaturated atmospheric conditions. This vapor pressure gradient ($e_a/e_i < 1$, Fig. S6c) contradicts with the theory of dew formation with vapor pressure gradient from atmosphere to the leaf/-canopy surfaces. These results indicated that estimation of T_L using R-package "tealeaves", which is based on steady-state leaf energy budget under well-controlled conditions (Muir, 2019), is difficult to support under a dynamic environment (Vialet-Chabrand and Lawson, 2019). With NRW inputs, the leaf energy balance is most likely very dynamic, hence there could be a delay to reach new thermal equilibrium between leaves and their environment (Vialet-Chabrand and Lawson, 2019). Assuming steady-state leaf energy budget could thus over-estimate leaf temperature during NRW nights with the leaf being cooler than air. High time resolution thermal imaging could be very helpful to simulate the dynamic leaf energy balance (Vialet-Chabrand and Lawson, 2019), but is not possible in our study with only one thermal image over a NRW night. Continuous thermal imaging will also allow to assess the changes of among-species leaf temperature differences, which was simply assumed constant in this study.

If among-species leaf temperature difference was considered, *Lolium* leaf with lower temperature than the average canopy temperature would experience earlier switch of air–leaf water exchange direction (Fig. 8). Later switch of air–leaf water exchange direction could be expected for *Taraxacum* and *Trifolium* with their higher leaf temperature than canopy surface temperature; but due to their little temperature difference (≤ 0.3 °C) from canopy surface temperature, the switch time difference was shorter than 30-min between species, hence was not captured with 30-min simulations.

We note that our interpolation of leaf water content (W) assumed that it followed the same trends of leaf water isotope variability. However, the actual leaf water content might not keep the same pace as isotope dynamics. This can be seen from the varied leaf water potential (Fig. 7a) between *Lolium* and *Taraxacum*, whilst their isotope changes followed the similar trends (Fig. 4). Isotope exchange was determined by partial vapor pressure gradient of minor isotopologues ($^1H^2H^{16}O$ and $^1H_2^{18}O$) and leaf conductance, whilst leaf water content changes can be affected by air–leaf vapor pressure gradient and plant physiological controls (e.g., stomatal regulation, root–leaf water potential gradient, and soil–root water potential gradient).

We used 2-h intervals of leaf water isotopes to simulate leaf conductance using non-steady state leaf water enrichment modeling, whilst 30-min intervals are recommended following assumptions of short-term steady-state. However, during NRW nights in our study, the

30-min changes of Δ_L (exponentially interpolated into 30-min) for ^{18}O was 0.2 ‰ on average, which was smaller than the measurement error of IRMS system. Higher time resolutions of Δ_L would induce the term d$(W \cdot \Delta_L)$/dt close to zero, and thus simulated g_L would be close to zero (see the results of 30-min g_L simulation in Table S2).

Stable isotopes of oxygen are sensitive to important biological and atmospheric processes, hence they are used for leaf temperature simulations (Drake et al., 2020), qualitative stomatal conductance analysis (Siegwolf et al., 2021), and mesophyll conductance simulations (Ogée et al., 2018). Furthermore, oxygen isotopes of tree-ring cellulose can be used for reconstructing paleoclimate (Fan et al., 2021; Field et al., 2022; Nagavciuc et al., 2022). Yet, stomatal conductance estimates based on oxygen isotopes have recently been controversially discussed with some studies being in favor of the isotope approach while others are not (Guerrieri et al., 2022; Lin et al., 2022). Furthermore, we should mention that there are remaining uncertainties about the biophysical processes relevant to the isotope fractionation in leaf water (Cernusak et al., 2016) that need to be clarified in future research. Leaf water enrichment models became increasingly complex (Cernusak et al., 2016). This additional level of complexity in modeling approaches requires adequate observational benchmarks to evaluate them in sufficient detail and corroborate the added value of the increased level of detail in process representation.

5. Conclusions

Our results indicate that during dew and radiation fog occurrence at night, leaf water experienced different water isotope dynamics as compared to that on a windy night. Leaf water equilibrated with atmospheric water vapor after 3.5–5.5 h of NRW exposure as shown during the N2 night. The non-steady state leaf water enrichment model led to total leaf conductance estimates of between 25 and 62 mmol m^{-2} s^{-1} (21–67 mmol m^{-2} s^{-1} for leaf stomatal conductance) for different species, depending on the methods of leaf temperature simulation. Total leaf conductance varied among species due to differences in the biophysical controls of the leaves. Radiative cooling and leaf wetting with NRW inputs caused a switch of direction in the air–leaf net exchange flux from leaf-to-air to air-to-leaf. Air–leaf water exchange amount was estimated as 11–25% of the total NRW input amounts over a NRW night. Our results show evidence of the ecological relevance of radiative cooling and leaf wetting on land–atmosphere interactions in natural temperate grasslands under real-world conditions, which cannot be adequately simulated in laboratory experiments due to experimental chambers acting as heat traps. We thus suggest that NRW inputs can be an important factor in the surface energy and water balance, as well as for modulating the survival and growth of short-statured grassland species in many regions affected by a drier climate. Future research combining radiation measurement and synchronous thermal imaging can simulate dynamic leaf energy balance and water budget during NRW inputs.

Funding

This study was supported by the Swiss National Science Foundation (grant 175,733, IFDewS project).

Author contribution

YL, AR, WE, FA, and NB designed the project. YL and AR performed the field experiment. YL carried out the laboratory work. YL performed all statistical analyses. FA, WE, and NB commented on the results of the data analysis. YL wrote and revised the manuscript, with contributions and feedbacks by FA, WE, NB, AR, LAC, MML, and RAW. WE passed away on 23 May 2022 before the final submission of this study.

Data availability

The data was deposited at ETH Zurich research collection 10.3929/ethz-b-000501244.

Declaration of Competing Interest

The authors declare that they have no known competing financial interests or personal relationships that could have appeared to influence the work reported in this paper.

Data Availability

I have shared the link in the paper.

Acknowledgments

The Picarro L2130-i analyzer was provided by the Atmospheric Dynamics group (Prof. Dr. Heini Wernli) at ETH Zurich. We thank Iris Feigenwinter, ETH Zurich, for the quality check of EC and meteorological data as well as LAI measurements; Dr. Kathrin Fuchs, KIT Garmisch-Partenkirchen (Germany), for her introduction to the Chamau field site; Dr. Lukas Hörtnagl, ETH Zurich, for the introduction to EC data analysis to YL; Dr. Anna Katarina Gilgen for her recommendation to select representative plant species. We thank the staff members of the Agricultural Education and Advice Center (LBBZ), Chamau, for their support with logistical and infrastructural aspects of this study. In addition, we thank Jim Ehleringer (University of Utah) for his valuable input on the discussions with YL.

Supplementary materials

Supplementary material associated with this article can be found, in the online version, at doi:10.1016/j.agrformet.2022.109256.

References

Aemisegger, F., Sturm, P., Graf, P., Sodemann, H., Pfahl, S., Knohl, A., Wernli, H., 2012. Measuring variations of $\delta^{18}O$ and $\delta^{2}H$ in atmospheric water vapour using two commercial laser-based spectrometers: an instrument characterisation study. Atmos. Meas. Tech. 5 (7), 1491–1511. https://doi.org/10.5194/amt-5-1491-2012.

Agam, N., Berliner, P.R., 2006. Dew formation and water vapor adsorption in semi-arid environments - a review. J. Arid Environ. 65 (4), 572–590. https://doi.org/10.1016/j.jaridenv.2005.09.004.

Arkebauer, T.J., 2005. Leaf Radiative Properties and the Leaf Energy Budget. Micrometeorology in Agricultural Systems, pp. 93–103. https://doi.org/10.2134/agronmonogr47.c5.

Aubinet, M., Vesala, T., Papale, D., 2012. Eddy covariance: a Practical Guide to Measurement and Data Analysis. Springer, Dordrecht, p. 438. https://doi.org/10.1007/978-94-007-2351-1.

Barnard, R.L., de Bello, F., Gilgen, A.K., Buchmann, N., 2006. The $\delta^{18}O$ of root crown water best reflects source water $\delta^{18}O$ in different types of herbaceous species. Rapid Commun. Mass Spectrom. 20 (24), 3799–3802. https://doi.org/10.1002/rcm.2778.

Barrs, H.D., Weatherley, P.E., 1962. A re-examination of the relative turgidity technique for estimating water deficits in leaves. Aust. J. Biol. Sci. 15 (3), 413–428. https://doi.org/10.1071/BI9620413.

Berry, Z.C., Emery, N.C., Gotsch, S.G., Goldsmith, G.R., 2018. Foliar water uptake: processes, pathways, and integration into plant water budgets. Plant Cell Environ. 42 (2), 410–423. https://doi.org/10.1111/pce.13439.

Bollig, C., Feller, U., 2014. Impacts of drought stress on water relations and carbon assimilation in grassland species at different altitudes. Agric. Ecosyst. Environ. 188, 212–220. https://doi.org/10.1016/j.agee.2014.02.034.

Bonan, G.B., Williams, M., Fisher, R.A., Oleson, K.W., 2014. Modeling stomatal conductance in the earth system: linking leaf water-use efficiency and water transport along the soil–plant–atmosphere continuum. Geosci. Model Dev. 7 (5), 2193–2222. https://doi.org/10.5194/gmd-7-2193-2014.

Boucher, J.F., Munson, A.D., Bernier, P.Y., 1995. Foliar absorption of dew influences shoot water potential and root-growth in pinus-strobus seedlings. Tree Physiol. 15 (12), 819–823. https://doi.org/10.1093/treephys/15.12.819.

Caird, M.A., Richards, J.H., Donovan, L.A., 2007. Nighttime stomatal conductance and transpiration in C_3 and C_4 plants. Plant Physiol. 143 (1), 4–10. https://doi.org/10.1104/pp.106.092940.

Cape, J.N., 1983. Contact angles of water droplets on needles of scots pine (*pinus-sylvestris*) growing in polluted atmospheres. New Phytol. 93 (2), 293–299. https://doi.org/10.1111/j.1469-8137.1983.tb03432.x.

Cernusak, L.A., Barbour, M.M., Arndt, S.K., Cheesman, A.W., English, N.B., Feild, T.S., Helliker, B.R., Holloway-Phillips, M.M., Holtum, J.A.M., Kahmen, A., McInerney, F. A., Munksgaard, N.C., Simonin, K.A., Song, X., Stuart-Williams, H., West, J.B., Farquhar, G.D., 2016. Stable isotopes in leaf water of terrestrial plants. Plant Cell Environ. 39 (5), 1087–1102. https://doi.org/10.1111/pce.12703.

Cernusak, L.A., Pate, J.S., Farquhar, G.D., 2002. Diurnal variation in the stable isotope composition of water and dry matter in fruiting Lupinus angustifolius under field conditions. Plant Cell Environ. 25 (7), 893–907. https://doi.org/10.1046/j.1365-3040.2002.00875.x.

Cernusak, L.A., Ubierna, N., Jenkins, M.W., Garrity, S.R., Rahn, T., Powers, H.H., Hanson, D.T., Sevanto, S., Wong, S.C., McDowell, N.G., Farquhar, G.D., 2018. Unsaturation of vapour pressure inside leaves of two conifer species. Sci. Rep. 8 https://doi.org/10.1038/s41598-018-25838-2.

CH2018, 2018. CH2018 – Climate scenarios for Switzerland, technical report, National Centre for Climate Services, Zurich. available at https://www.nccs.admin.ch/nccs/en/home/climate-change-and-impacts/swiss-climate-change-scenarios/technical-report.html (last access 1st June 2021).

Criss, R.E., 1999. Principles of Stable Isotope Distribution. Oxford University Press, New York, Oxford. https://doi.org/10.1093/oso/9780195117752.001.0001.

Curtis, O.F., 1936. Leaf temperatures and the cooling of leaves by radiation. Plant Physiol. 11 (2), 343–364. https://doi.org/10.1104/pp.11.2.343.

Dawson, T.E., 1998. Fog in the California redwood forest: ecosystem inputs and use by plants. Oecologia 117 (4), 476–485. https://doi.org/10.1007/s004420050683.

Dawson, T.E., Ehleringer, J.R., 1991. Streamside trees that do not use stream water. Nature 350 (6316), 335–337. https://doi.org/10.1038/350335a0.

Dawson, T.E., Goldsmith, G.R., 2018. The value of wet leaves. New Phytol. 219 (4), 1156–1169. https://doi.org/10.1111/nph.15307.

Drake, J.E., et al., 2020. No evidence of homeostatic regulation of leaf temperature in Eucalyptus parramattensis trees: integration of CO_2 flux and oxygen isotope methodologies. New Phytol. 228 (5), 1511–1523. https://doi.org/10.1111/nph.16733.

Ehleringer, J.R., Dawson, T.E., 1992. Water-uptake by plants - perspectives from stable isotope composition. Plant Cell Environ. 15 (9), 1073–1082. https://doi.org/10.1111/j.1365-3040.1992.tb01657.x.

Eller, C.B., Lima, A.L., Oliveira, R.S., 2013. Foliar uptake of fog water and transport belowground alleviates drought effects in the cloud forest tree species, *Drimys brasiliensis* (Winteraceae). New Phytol. 199 (1), 151–162. https://doi.org/10.1111/nph.12248.

Fan, R., Shimada, H., Tei, S., Maximov, T.C., Sugimoto, A., 2021. Oxygen isotope compositions of cellulose in earlywood of larix cajanderi determined by water source rather than leaf water enrichment in a permafrost ecosystem, Eastern Siberia. J. Geophys. Res. Biogeosci. 126 (9), e2020JG006125 https://doi.org/10.1029/2020JG006125.

Farquhar, G.D., Cernusak, L.A., 2005. On the isotopic composition of leaf water in the non-steady state. Funct. Plant Biol. 32 (4), 293–303. https://doi.org/10.1071/fp04232.

Farquhar, G.D., Lloyd, J., 1993. Carbon and oxygen isotope effects in the exchange of carbon dioxide between terrestrial plants and the atmosphere. J.R. Ehleringer, A.E. Hall and G.D. Farquhar (Editors Stable Isotopes and Plant Carbon-Water Relations. Academic Press, San Diego, pp. 47–70. https://doi.org/10.1016/B978-0-08-091801-3.50011-8.

Field, R.D., et al., 2022. Tree-ring cellulose δ18O records similar large-scale climate influences as precipitation δ18O in the Northwest Territories of Canada. Clim. Dyn. 58 (3), 759–776. https://doi.org/10.1007/s00382-021-05932-4.

Feild, T.S., Dawson, T.E., 1998. Water sources used by Didymopanax pittieri at different life stages in a tropical cloud forest. Ecology 79 (4), 1448–1452. https://doi.org/10.1890/0012-9658(1998)079[1448:wsubdp]2.0.co;2.

Fernandez, V., Sancho-Knapik, D., Guzman, P., Javier Peguero-Pina, J., Gil, L., Karabourniotis, G., Khayet, M., Fasseas, C., Heredia-Guerrero, J.A., Heredia, A., Gil-Pelegrin, E., 2014. Wettability, polarity, and water absorption of holm oak leaves: effect of leaf side and age. Plant Physiol. 166 (1), 168–180. https://doi.org/10.1104/pp.114.242040.

Foster, J.R., Smith, W.K., 1986. Influence of stomatal distribution on transpiration in low-wind environments. Plant Cell Environ. 9 (9), 751–759. https://doi.org/10.1111/j.1365-3040.1986.tb02108.x.

Fricke, W., Akhiyarova, G., Veselov, D., Kudoyarova, G., 2004. Rapid and tissue-specific changes in ABA and in growth rate in response to salinity in barley leaves. J. Exp. Bot. 55 (399), 1115–1123. https://doi.org/10.1093/jxb/erh117.

Fuchs, K., Hörtnagl, L., Buchmann, N., Eugster, W., Snow, V., Merbold, L., 2018. Management matters: testing a mitigation strategy for nitrous oxide emissions using legumes on intensively managed grassland. Biogeosciences 15 (18), 5519–5543. https://doi.org/10.5194/bg-15-5519-2018.

Gat, J.R., 1981. Stable Isotope Hydrology: Deuterium and Oxygen-18 in the Water Cycle. IAEA, International Atomic Energy Agency (IAEA) available at. https://inis.iaea.org/collection/NCLCollectionStore/_Public/13/677/13677657.pdf?r=1 (last access 1st June 2021).

Gerlein-Safdi, C., Gauthier, P.P.G., Caylor, K.K., 2018. Dew-induced transpiration suppression impacts the water and isotope balances of Colocasia leaves. Oecologia 187 (4), 1041–1051. https://doi.org/10.1007/s00442-018-4199-y.

Goldsmith, G.R., Lehmann, M.M., Cernusak, L.A., Arend, M., Siegwolf, R.T.W., 2017. Inferring foliar water uptake using stable isotopes of water. Oecologia 184 (4), 763–766. https://doi.org/10.1007/s00442-017-3917-1.

Groh, J., Putz, T., Gerke, H.H., Vanderborght, J., Vereecken, H., 2019. Quantification and prediction of nighttime evapotranspiration for two distinct grassland ecosystems. Water Resour. Res. 55 (4), 2961–2975. https://doi.org/10.1029/2018wr024072.

Guerrieri, R., et al., 2022. Detecting long-term changes in stomatal conductance: challenges and opportunities of tree-ring δ18O proxy. New Phytol. 236 (3), 809–812. https://doi.org/10.1111/nph.18430.

Gutschick, V.P., 2016. Leaf energy balance: basics, and modeling from leaves to canopies, Canopy photosynthesis: from basics to applications. Springer 23–58. https://doi.org/10.1007/978-94-017-7291-4_2.

Helliker, B.R., Griffiths, H., 2007. Toward a plant-based proxy for the isotope ratio of atmospheric water vapor. Glob. Change Biol. 13 (4), 723–733. https://doi.org/10.1111/j.1365-2486.2007.01325.x.

Holder, C.D., 2007. Leaf water repellency of species in Guatemala and Colorado (USA) and its significance to forest hydrology studies. J. Hydrol. 336 (1–2), 147–154. https://doi.org/10.1016/j.jhydrol.2006.12.018 (Amst).

Horita, J., Wesolowski, D.J., 1994. Liquid-vapor fractionation of oxygen and hydrogen isotopes of water from the freezing to the critical temperature. Geochim. Cosmochim. Acta 58 (16), 3425–3437. https://doi.org/10.1016/0016-7037(94)90096-5.

IAEA, 2009. Reference Sheet For VSMOW2 and SLAP2 International Measurement Standards. International Atomic Energy Agency (IAEA), Vienna, Austria, p. 8.

IPCC, 2021. Climate Change 2021: the Physical science basis. Contribution of Working Group I to the sixth assessment report of the intergovernmental panel on climate change. available at: https://www.ipcc.ch/report/ar6/wg1/(last access on 8th September 2021).

Jacobs, A.F.G., Heusinkveld, B.G., Kruit, R.J.W., Berkowicz, S.M., 2006. Contribution of dew to the water budget of a grassland area in the Netherlands. Water Resour. Res. 42 (3), W03415. https://doi.org/10.1029/2005WR004055.

Kahmen, A., Simonin, K., Tu, K., Goldsmith, G.R., Dawson, T.E., 2009. The influence of species and growing conditions on the 18-O enrichment of leaf water and its impact on 'effective path length'. New Phytol. 184 (3), 619–630. https://doi.org/10.1111/j.1469-8137.2009.03008.x.

Kaseke, K.F., Wang, L.X., Seely, M.K., 2017. Nonrainfall water origins and formation mechanisms. Sci. Adv. 3 (3), e1603131 https://doi.org/10.1126/sciadv.1603131.

Kerr, J.P., Beardsell, M.F., 1975. Effect of dew on leaf water potentials and crop resistances in a paspalum pasture. Agron. J. 67 (5), 596–599. https://doi.org/10.2134/agronj1975.00021962006700050002x.

Kim, K., Lee, X., 2011. Transition of stable isotope ratios of leaf water under simulated dew formation. Plant Cell Environ. 34 (10), 1790–1801. https://doi.org/10.1111/j.1365-3040.2011.02375.x.

Lai, C.T., Ometto, J.P., Berry, J.A., Martinelli, L.A., Domingues, T.F., Ehleringer, J.R., 2008. Life form-specific variations in leaf water oxygen-18 enrichment in Amazonian vegetation. Oecologia 157 (2), 197–210. https://doi.org/10.1007/s00442-008-1071-5.

Lee, X., Griffis, T.J., Baker, J.M., Billmark, K.A., Kim, K., Welp, L.R., 2009. Canopy-scale kinetic fractionation of atmospheric carbon dioxide and water vapor isotopes. Glob. Biogeochem. Cycles 23 (1). https://doi.org/10.1029/2008GB003331.

Lehmann, M.M., Goldsmith, G.R., Mirande-Ney, C., Weigt, R.B., Schonbeck, L., Kahmen, A., Gessler, A., Siegwolf, R.T.W., Saurer, M., 2020. The ^{18}O-signal transfer from water vapour to leaf water and assimilates varies among plant species and growth forms. Plant Cell Environ. 43 (2), 510–523. https://doi.org/10.1111/pce.13682.

Lehmann, M.M., Goldsmith, G.R., Schmid, L., Gessler, A., Saurer, M., Siegwolf, R.T.W., 2018. The effect of ^{18}O-labelled water vapour on the oxygen isotope ratio of water and assimilates in plants at high humidity. New Phytol. 217 (1), 105–116. https://doi.org/10.1111/nph.14788.

Li, D., Li, X., Xi, B., Hernandez-Santana, V., 2022. Evaluation of method to model stomatal conductance and its use to assess biomass increase in poplar trees. Agric. Water Manag. 259, 107228. https://doi.org/10.1016/j.agwat.2021.107228.

LI-COR, 2019. Eddy Covariance Processing Software (Version 7.0.6) [Software]. LI-COR. LI-COR, Inc. https://www.licor.com/env/products/eddy_covariance/software.html.

Li, Y., Aemisegger, F., Riedl, A., Buchmann, N., Eugster, W., 2021. The role of dew and radiation fog inputs in the local water cycling of a temperate grassland during dry spells in central. Europe. Hydrol. Earth Syst. Sci. 25 (5), 2617–2648. https://doi.org/10.5194/hess-25-2617-2021.

Lin, W., Barbour, M.M., Song, X., 2022. Do changes in tree-ring δ18O indicate changes in stomatal conductance? New Phytol. 236 (3), 803–808. https://doi.org/10.1111/nph.18431.

López, A., Molina-Aiz, F.D., Valera, D.L., Peña, A., 2012. Determining the emissivity of the leaves of nine horticultural crops by means of infrared thermography. Sci. Hortic. 137, 49–58. https://doi.org/10.1016/j.scienta.2012.01.022.

Merlivat, L., 1978. Molecular diffusivities of $H_2^{16}O$, $HD^{16}O$, and $H_2^{18}O$ in gases. J. Chem. Phys. 69 (6), 2864–2871. https://doi.org/10.1063/1.436884.

Monteith, J.L., 1957. Dew. Q. J. R. Meteorol. Soc. 83 (357), 322–341. https://doi.org/10.1002/qj.49708335706.

Muir, C.D., 2019. tealeaves: an R package for modelling leaf temperature using energy budgets. AoB Plants 11 (6). https://doi.org/10.1093/aobpla/plz054.

Nagavciuc, V., Ionita, M., Kern, Z., McCarroll, D., Popa, I., 2022. A ~700 years perspective on the 21st century drying in the eastern part of Europe based on δ18O in tree ring cellulose. Commun. Earth Environ. 3 (1), 277. https://doi.org/10.1038/s43247-022-00605-4.

Ogée, J., Wingate, L., Genty, B., 2018. Estimating mesophyll conductance from measurements of C18OO photosynthetic discrimination and carbonic anhydrase activity. Plant Physiol. 178 (2), 728–752. https://doi.org/10.1104/pp.17.01031.

Ogle, K., Lucas, R.W., Bentley, L.P., Cable, J.M., Barron-Gafford, G.A., Griffith, A., Ignace, D., Jenerette, G.D., Tyler, A., Huxman, T.E., Loik, M.E., Smith, S.D., Tissue, D.T., 2012. Differential daytime and night-time stomatal behavior in plants from North American deserts. New Phytol. 194 (2), 464–476. https://doi.org/10.1111/j.1469-8137.2012.04068.x.

Pearcy, R.W., Schulze, E.D., Zimmermann, R., 1989. Measurement of transpiration and leaf conductance. R.W. Pearcy, J.R. Ehleringer, H.A. Mooney and P.W. Rundel (Editors). Plant Physiological Ecology: Field methods and Instrumentation. Springer Netherlands, Dordrecht, pp. 137–160. https://doi.org/10.1007/978-94-009-2221-1_8.

Pina, A.L.C.B., Zandavalli, R.B., Oliveira, R.S., Martins, F.R., Soares, A.A., 2016. Dew absorption by the leaf trichomes of Combretum leprosum in the Brazilian semiarid region. Funct. Plant Biol. 43 (9), 851–861. https://doi.org/10.1071/fp15337.

Prechsl, U.E., Burri, S., Gilgen, A.K., Kahmen, A., Buchmann, N., 2015. No shift to a deeper water uptake depth in response to summer drought of two lowland and subalpine C_3-grasslands in Switzerland. Oecologia 177 (1), 97–111. https://doi.org/10.1007/s00442-014-3092-6.

Prechsl, U.E., Gilgen, A.K., Kahmen, A., Buchmann, N., 2014. Reliability and quality of water isotope data collected with a lowbudget rain collector. Rapid Commun. Mass Spectrom. 28 (8), 879–885. https://doi.org/10.1002/rcm.6852.

Core Team, R., 2021. R: A Language and Environment For Statistical Computing. R Foundation for Statistical Computing, Vienna, Austria.

Riedl, A., Li, Y., Eugster, J., Buchmann, N., Eugster, W., 2022. Technical note: high-accuracy weighing micro-lysimeter system for long-term measurements of non-rainfall water inputs to grasslands. Hydrol. Earth Syst. Sci. 2021, 1–34. https://doi.org/10.5194/hess-26-91-2022.

Roth K., 2006. Bodenkartierung und GIS-basierte Kohlenstoffinventur von Graslandböden: Untersuchungen an den ETH-Forschungsstationen Chamau und Früebüel (ZG, Schweiz) (in German). Diploma thesis Thesis, University of Zurich, Switzerland.

Saxton, K.E., Rawls, W.J., Romberger, J.S., Papendick, R.I., 1986. Estimating generalized soil-water characteristics from texture. Soil Sci. Soc. Am. J. 50 (4), 1031–1036. https://doi.org/10.2136/sssaj1986.03615995005000040039x.

Schonherr, J., Bukovac, M.J., 1972. Penetration of stomata by liquids - dependence on surface-tension, wettability, and stomatal morphology. Plant Physiol. 49 (5), 813. https://doi.org/10.1104/pp.49.5.813. -+.

Schreel, J.D.M., Steppe, K., 2020. Foliar water uptake in trees: negligible or necessary? Trends Plant Sci. 25 (6), 590–603. https://doi.org/10.1016/j.tplants.2020.01.003.

Schymanski, S.J., Or, D., 2017. Leaf-scale experiments reveal an important omission in the Penman–Monteith equation. Hydrol. Earth Syst. Sci. 21 (2), 685–706. https://doi.org/10.5194/hess-21-685-2017.

Stohler A., 2006. Auswirkungen von Trockenheit auf die Bestandesstruktur von Wiesen (Effects of drought on the stand structure of meadows). Diploma thesis Thesis, ETH Zurich, Switzerland.

Siegwolf, R., Lehmann, M., Goldsmith, G., Churakova, O., Mirande-Ney, C., Gruspante, G., Saurer, M., 2021. The dual C and O isotope–gas exchange model: A concept review for understanding plant responses to the environment and its application in tree rings. Authorea Preprints. https://doi.org/10.22541/au.163844646.68129291/v1.

Stull, R.B., 1988. Stable boundary layer. R.B. Stull (Editor). An Introduction to Boundary Layer Meteorology. Springer, Dordrecht, Dordrecht, pp. 499–543. https://doi.org/10.1007/978-94-009-3027-8_12.

Thurnherr, I., Kozachek, A., Graf, P., Weng, Y.B., Bolshiyanov, D., Landwehr, S., Pfahl, S., Schmale, J., Sodemann, H., Steen-Larsen, H.C., Toffoli, A., Wernli, H., Aemisegger, F., 2020. Meridional and vertical variations of the water vapour isotopic composition in the marine boundary layer over the Atlantic and Southern Ocean. Atmos. Chem. Phys. 20 (9), 5811–5835. https://doi.org/10.5194/acp-20-5811-2020.

Urey, H.C., 1947. The thermodynamic properties of isotopic substances. J. Chem. Soc. 562–581. https://doi.org/10.1039/jr9470000562 (May).

Vesala, T., Sevanto, S., Gronholm, T., Salmon, Y., Nikinmaa, E., Hari, P., Holtta, T., 2017. Effect of leaf water potential on internal humidity and CO_2 dissolution: reverse transpiration and improved water use efficiency under negative pressure. Front. Plant Sci. 8, 54. https://doi.org/10.3389/fpls.2017.00054.

Vialet-Chabrand, S., Lawson, T., 2019. Dynamic leaf energy balance: deriving stomatal conductance from thermal imaging in a dynamic environment. J. Exp. Bot. 70 (10), 2839–2855. https://doi.org/10.1093/jxb/erz068.

Wang, X.F., Yakir, D., Avishai, M., 1998. Non-climatic variations in the oxygen isotopic compositions of plants. Glob. Change Biol. 4 (8), 835–849. https://doi.org/10.1046/j.1365-2486.1998.00197.x.

Welp, L.R., Lee, X., Kim, K., Griffis, T.J., Billmark, K.A., Baker, J.M., 2008. $\delta^{18}O$ of water vapour, evapotranspiration and the sites of leaf water evaporation in a soybean canopy. Plant Cell Environ. 31 (9), 1214–1228. https://doi.org/10.1111/j.1365-3040.2008.01826.x.

Wen, X.F., Lee, X., Sun, X.M., Wang, J.L., Hu, Z.M., Li, S.G., Yu, G.R., 2012. Dew water isotopic ratios and their relationships to ecosystem water pools and fluxes in a cropland and a grassland in China. Oecologia 168 (2), 549–561. https://doi.org/10.1007/s00442-011-2091-0.

Wong, S.C., Canny, M.J., Holloway-Phillips, M., Stuart-Williams, H., Cernusak, L.A., Marquez, D.A., Farquhar, G.D., 2022. Humidity gradients in the air spaces of leaves. Nat Plants 8 (8), 971. https://doi.org/10.1038/s41477-022-01202-1.

Yu, L., Wang, W., Zhang, X., Zheng, W., 2015. A review on leaf temperature sensor: measurement methods and application, International conference on computer and computing technologies in agriculture. Springer 216–230. https://doi.org/10.1007/978-3-319-48357-3_21.